Electro-kinetically Enhanced Nano-metric Material Removal

A Thesis Presented to the Academic Faculty

By

Travis Lee Blackburn

In Partial Fulfillment
of the Requirements for the Degree
Master of Science in the
School of Mechanical Engineering

Acknowledgements

There have been a multitude of individuals who have helped me along the way with this project. Although it is impossible to include everyone, I will do my best. First of all, I would like to thank my advisor, Dr. Steven Danyluk. Dr. Danyluk has provided guidance, patience, and support through this strenuous process. His technical knowledge has been a huge benefit as I grew to understand the concepts and mechanisms governing my work. The countless hours that he spent discussing concepts and offering suggestions on the direction of my work were priceless. Also, the time he spent reading and correcting my thesis have vastly improved my technical writing skills. I also would like to thank Dr. Danyluk for sending me to Singapore to perform my research. This experience has not only benefited me educationally and professionally, but socially. The cultural experience of living overseas for ten months will be something I carry with me for the rest of my life.

I also would like to thank Dr. David Butler, who acted as my advisor while I was at Nanyang Technological University (NTU) in Singapore. Dr. Butler not only provided guidance and support on my project, he also helped me to become acclimated to living in a new country. He trained me on numerous types of metrology equipment that was crucial for analysis of my results. Dr. Butler was always available any time I had a concern that needed to be addressed. The knowledge and generosity that Dr. Butler shared with me throughout this project have benefited me as an engineer and as a person.

I would also like to thank Dr. Yang Chun (Charles), associate professor at NTU. He and I spent many hours discussing micro-fluidic and electro-kinetic concepts which led to the realization of my mathematical model. Dr. Yang was very active throughout

the project helping to understand the mechanisms behind our material removal approach. Along the same lines, I would like to thank Dr. Ng Sum Huan (Gary) of the Singapore Institute of Manufacturing Technology (SimTech). Dr. Ng is a former student of Dr. Danyluk and his previous work greatly influenced the direction of this project. Gary helped with the original design concept and fabrication of the micro-fluidic device. He provided many of the resources that were required to complete the project. I also would like to thank him for the many technical conversations that he had with me while I was performing my research. I would also like to thank two other professors, Dr. Peter Hesketh and Dr. Minami Yoda, for agreeing to be on my masters thesis committee. Their patience and suggestions have been un-measureable in completing my thesis.

One of the most important people I need to thank is Leo Cheng Seng, a masters student of Dr. Butler's at NTU. Cheng Seng and I worked hand in hand on this project. He and I constantly bounced ideas off of one another and discussed key concepts which led to the development of a non-contact nano-metric material removal approach. Cheng Seng spent countless hours helping with the fabrication of the micro-fluidic device. His fresh ideas and vast knowledge greatly enhanced the quality of my work. I cannot imagine having worked with a better student than Cheng Seng on this project and I'm greatly appreciative of all of his support. Cheng Seng is continuing my work in this field and I look for additional impressive results out of him in the future.

Many thanks go out NTU and SimTech for allowing me to perform my research in Singapore and for providing all of the necessary resources for completing this project. I would like to thank Tan-Ong Pek, technician in the metrology lab at NTU, for handing all of my purchase orders. My appreciation also goes out to Lisa Teasley, administrative

assistant to Dr. Danyluk at Georgia Tech, for scheduling my appointments with Dr. Danyluk and providing any additional resources that I needed. Gratitude should also be extended to Glenda Johnson, mechanical engineering academic advisor at Georgia Tech, who helped make since of the confusing administrative tasks that go into submitting a thesis.

I would like to offer special thanks to the members of Dr. Butler's metrology lab group, Ho Shook Foong (Jessica), Toh Guek Geok (Alicia), and Kitamura Mariko. These girls not only provided me with individuals to exchange ideas with during my research process but they also helped me to get acclimated to living in Singapore. My transition would not have been nearly as smooth without their support, and for that I thank them. I would also like to thank my lab mates at Georgia Tech, Frank Mess, Sergey Tsiareshka, Fang Li, Yury Pyekh, Vicky Garcia, and Megan Dukic for their support and feedback during this process.

Lastly, I would like to thank my friends and family for their support. I could not ask for a better supporting cast in dealing with the emotional stress that comes with completing a masters thesis. My friends and family provided a shoulder to lean on anytime I encountered frustrating problems or difficulties acclimating to a different country. I will always remember them when I think back on this time.

Table of Contents

List of Tables

List of Figures

Chapter 1: Introduction

The further development of miniaturized semiconductor devices requires short device node and lower-k dielectrics in order to reduce the gate and interconnect delay times. In the past, chemical mechanical planarization (CMP) techniques have been widely used for removing uneven topography in the multilevel metallization process. CMP was first developed by IBM in the 1980s in order to produce flat surfaces on silicon wafer substrates or partially-processed wafers during the manufacturing of integrated circuits (IC's). CMP has been very successful in meeting the demand for dimensional accuracy of devices in the micrometer (10^{-6} m) range. However, as demand has shifted to dimensional accuracy of devices in the nanometer (10^{-9} m) and angstrom (10^{-10} m) range conventional CMP techniques face problems. CMP is a high downforce-dependent process which causes excessive amounts of dishing and erosion, resulting in high electrical resistance across various pattern densities. Also, high downforce-dependent processes tend to cause mechanical failures in fragile low-k dielectrics.

Several techniques have been developed to meet the need for miniaturization with minimal defects. These techniques will be explained in detail in Chapter 2. One such technique is electrochemical CMP, which is a high removal rate process that minimizes downforce and uses an applied voltage to control removal rate. Also, ultra-precision polishing has gained attraction for producing geometrically dimensional surface features in the nanometer range. This process is able to produce a very smooth surface with minimal damage and strain which is a fundamental requirement for miniaturized functional semiconductor components. Recently, non-contact ultra-precision polishing techniques have generated interest because these processes eliminate polishing tool-

work-piece interaction which can lead to defects such as scratching on the work-piece surface. Two processes which fall under non-contact ultraprecision techniques are float polishing and elastic emission machining. These processes use slurries containing abrasive particles suspended in fluid to remove material from a work-piece surface.

The purpose of this thesis is to investigate an ultra-precision material removal technique based on the electro-kinetic phenomenon with the desire of enhancing planarization performance. The goal is to prove the concept that electric field-activated abrasive particles in solution can remove metallic material from a silicon wafer test substrate. The objective of this thesis is to validate three concepts:

1. Abrasive particles in solution can be influenced and controlled by changes in electric field.
2. Abrasive particles controlled by an electric field can remove metallic material from a test substrate.
3. Changes in electric field can control the amount of metallic material removed from the test substrate in a given amount of time.

A micro-fluidic device was designed and fabricated in order to prove the preceding concepts. The following chapters of this thesis will provide a literature review of the techniques and concepts which led to the development of the electo-kinetic nanometric material removal process followed by a detailed description of the development of the process. A mathematical model predicting the removal rate of metallic material from a silicon wafer test substrate will also be presented and compared with the experimental material removal rates.

Chapter 2: Literature Review

2.1 Material Removal Processes

Chemical mechanical planarization (CMP) has been the preferred planarization step in deep sub-micron IC fabrication. CMP is a process that can remove topography from silicon oxide, metal and polysilicon surfaces. Essentially, CMP is the process of smoothing surfaces through the combination of chemical and mechanical forces. It employs a combination of concepts from chemical etching and free abrasive polishing. Mechanical grinding of surfaces alone may produce desired planarization but the process produces significant surface damage. Chemistry alone also cannot attain planarization because most chemical reactions are anisotropic. Therefore, the planarization achieved with the CMP process cannot be explained solely by the individual physical and chemical effects. CMP also utilizes the fact that high points on a wafer surface are subjected to higher pressures from the pad which enhances the material removal rates in those areas [1].

CMP has most widely been utilized in back-end IC manufacturing. These processes involve using thin layers of metal and dielectric materials to form electrical interconnections between IC components. Interconnects are formed by depositing thin films of materials and removing or changing the properties of the material in certain areas. CMP is used in the interconnect process to planarize step heights caused by depositing thin films over existing features so that levels can be added to the planarized surface. [2,3] CMP has faced challenges producing the desired planarization necessary for interconnect technology without causing surface damage. Pan *et al* [4] reported problems during the process of removing overburden copper deposited above the

dielectric surface. During the copper CMP process, a degree of over-polish has to be used to remove metallic material from the dielectric surface to ensure electrical isolation between adjacent circuits. The over-polish required to remove the metallic material has been reported to cause copper dishing and oxide erosion. Dishing and erosion are also reported to be a function of surface feature size and pattern density. The problems associated with copper dishing and oxide erosion include deviation from the desired line resistance required due to copper thickness loss and excess surface topography which complicates the fabrication of the next metal layer.

The concept for the nano-metric material removal process investigated in this thesis was partially developed from research performed on langasite polishing and electrochemical mechanical planarization techniques [5]. Both of these techniques employ variations of the typical CMP process in order to increase material removal rates while limiting surface damage effects. Grover *et al* [6] reported that increasing the material removal rate without generating surface damage is difficult because CMP is a complex process involving chemical and mechanical interactions between the polishing pad, slurry, and substrate material. Therefore, techniques have been developed which employ DC potentials into the polishing process to increase wear rate.

Lim *et al* [5] investigated the effect of DC electric fields on material removal rates of single crystal langasite during the CMP process. In this process, langasite wafers were sliced from a single crystal. The backside of the langasite wafers were electroplated with copper foil so that an electric field could be applied during polishing experiments. Electrical connections were made with the copper electrode and ground. A DC potential ranging from -300 to +300 V/mm was applied to these electrical connections during

polishing experiments. The polishing experiments enhanced by the DC electric field resulted in a 30% increase on material removal rates of the langasite crystal. The influence of the electric field was explained by the increased number of particles near the work-piece surface. It was found that that an increased number of abrasive silica particles were present near the langasite surface during the presence of a DC electric field. The study hypothesized that the polishing rate increased with the applied electric field because of the increase in the number of particles involved in the polishing process

This hypothesis made from prior work suggested that the presence of an electric field would increase the material removal rate because the hardness of the polishing surface decreased. Yost and Williams [7] suggested that by applying an electric field, the surface charge would weaken the surface bonds, decreasing the surface hardness making the generation of dislocations easier. However, the research by Lim concluded that the hardness of the langasite crystal was not affected by an applied electric field. Therefore, it was concluded that it was the slurry action which was modified by the electric field and affected the material removal rates, not the surface hardness.

Another promising alternative to the typical CMP process is electrochemical mechanical planarization (ECMP), which was developed by Applied Materials [8]. In electrochemical mechanical planarization (ECMP), an electrolyte chemistry with no or very low concentrations of abrasive slurry (colloidal particles) is used, and thus features high planarization efficiency. A DC electric potential instead of the oxidizer is the driving force to oxidize metal to metal ions. Metal ions can then react with components in electrolyte to either go in solution or form a passivation layer. A polishing pad is used to help achieve planarization. Since this passivation layer can be removed easily,

mechanical downforce is not a limiting factor to achieve high removal rate, enabling a virtually zero downforce (<3.5 kPa) planarization process that produced material removal rates exceeding 6,000 Å/min. The advantages of the electrochemical mechanical planarization include reduction of dishing, erosion, metal loss, enhancement of overall planarization performance, higher process stability and lower consumables required. In addition, since the electrochemical mechanical planarization can be performed using electrolytes with no or very low concentrations of abrasive particles, several disadvantages of conventional CMP associated with the use of slurries containing high concentrations of abrasive particles, such as lack of within-wafer uniformity, particle coagulation, slurry-handling and waste disposal are minimized or eliminated.

Non-contact ultra-precision polishing techniques have generated interest because these processes eliminate polishing tool-work-piece interaction which can lead to defects such as scratching on the work-piece surface. One such technique is elastic emission machining (EEM) [9,10] which is capable of machining silicon in the atomic order with minimal surface roughness. In EEM, ultra-fine powders such as SiO_2, Al_2O_3 and ZrO_2 with diameters much smaller than 1 μm are uniformly mixed with water to create a slurry. The slurry is accelerated and transported to a silicon work-piece surface using a rotating polyurethane sphere with an applied vertical load. The vertical load is optimized so that the sphere nearly comes into contact with the work-piece. This creates a fluid film thickness between the sphere and the work-piece of 1 μm, much larger than the diameters of the particles. The load and the fluid pressure are balanced to maintain a uniform film thickness, which enables a constant flow rate between the polyurethane sphere and the work-piece. This ensures that the slurry is transported without scratching

the surface. Before coming into contact, the ultra-fine powders and silicon work-piece react with water to form hydroxide species. When the particles are accelerated and transported into contact with the surface, hydrogen bonding occurs between the two surfaces. Because oxygen atoms have high electronegativity, silicon atoms on the work-piece surface are removed as the powders begin to separate from the work-piece surface. This mechanism produces atomic-level material removal from a silicon work-piece.

Another non-contact ultra-precision technique which has been employed for the fabrication of optical, electronic, and magnetic components with damage-free surfaces is float polishing [11,12]. The mechanism for removal of surface material is similar to that of EEM. In float polishing, a weighted sample and a lap are submerged in slurry containing DI water and polishing powder. The sample and the lap are rotated in the same circular direction and normally at the same rate. Under equilibrium, the sample floats on top of a fluid layer of approximately 1 μm above the lap and is bombarded by the polishing particles in the slurry. The removal mechanisms could be kinetic, chemical, diffusive, or a combination of all three. Material removal rates depend on several process variables including type of polishing powder, the sample, the lap materials, the groove pattern (removal areas), the rotational rates of the sample and the lap, and the sample loading. The polishing particles' diameter typically ranges from 1 nm for SiO_2 to 100 nm for TiO_2, Al_2O_3, CeO_2, and MgO. Soares *et al* [12] found that pressure gradients in the grooves cause the sample to float above the lap layer of the slurry and fluid flow is laminar which results in a high quality polish since the substrate is not in contact with the lap. The study concluded that subsurface damage was much lower for 100 μm material removal compared to 10 μm removal. Therefore, this process probably is not optimal for

producing nano-metric size geometric features on a substrate since smaller amounts of material removal led to more subsurface damage.

The previous techniques are all processes that are capable of removing nano-metric amounts of metallic material from substrates. The remainder of this thesis is devoted to presenting a non-contact nano-metric material removal technique based on the electrokinetic phenomenon.

2.2 Electro-kinetic Phenomena

In order to remove metallic material from a work-piece, abrasive, negatively charged silica particles have to be accelerated vertically through the micro-channel to the work-piece surface. The concept which governs this particle movement is the Electro-kinetic phenomenon. Electro-kinetic phenomena arise whenever relative movement occurs between a charged interface and the adjacent electrolyte solution, so that part of the double layer charge moves with the liquid. As the charged surface moves in the appropriate direction, ions in the mobile part of the double layer undergo a net migration in the opposite direction. Migration of the ions carries solvent along with it and an electric field is created if the charged surface and the diffuse part of the double layer move relative to each other. Electrophoresis is one type of phenomena that arises out of relative motion between charged phases and electrolytes. [13,14]

Electrophoresis is the movement of a charged surface, such as a colloidal silica particle, relative to a stationary liquid caused by an applied electric field [13,14]. Figure 1 is a schematic of electrophoresis of a charged particle in an external electric field. The presence of the anode and cathode terminals establishes an electric field from top to

bottom. The electric field causes a negatively charged colloidal particle to migrate toward the anode.

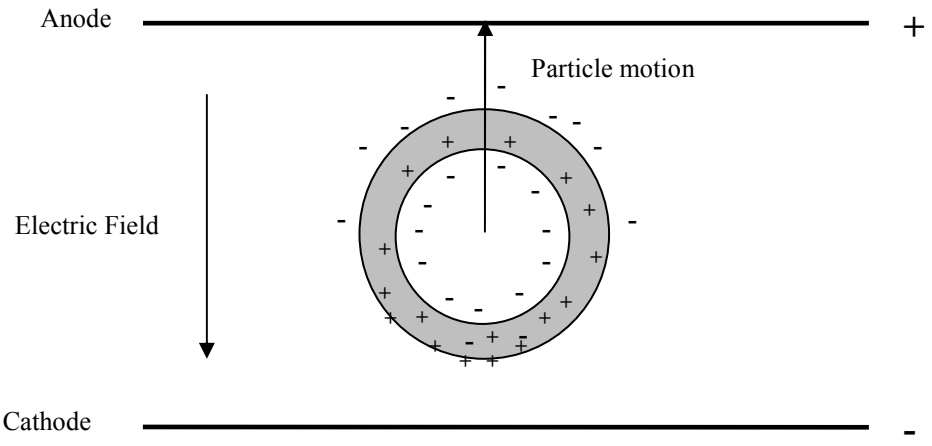

Figure 1. Electrophoresis of a charged particle in an external electric field [14]

The electrophoresis concept describes the motion of a charged particle in solution under the influence of an externally applied electric field. Later, this concept will be extended to describe the forces which act on the particle during electrophoresis. With the general motion of a negatively charged particle realized, the concept that these particles can be effectively controlled to remove metallic material from a work-piece surface has to be proved. In order to validate this concept, a micro-fluidic device was designed and fabricated.

Chapter 3: Micro-fluidic Device Design and Fabrication

A micro-fluidic device was designed and fabricated in order to validate the concept that the motion of electro-kinetically enhanced abrasive particles in solution can effectively be controlled to remove metallic layers deposited onto a silicon wafer. At the onset of the experiments, a general experimental configuration was designed in order to view the motion of particles in solution under the influence of electric field. Figure 2 shows the design of the device for visualization experiments.

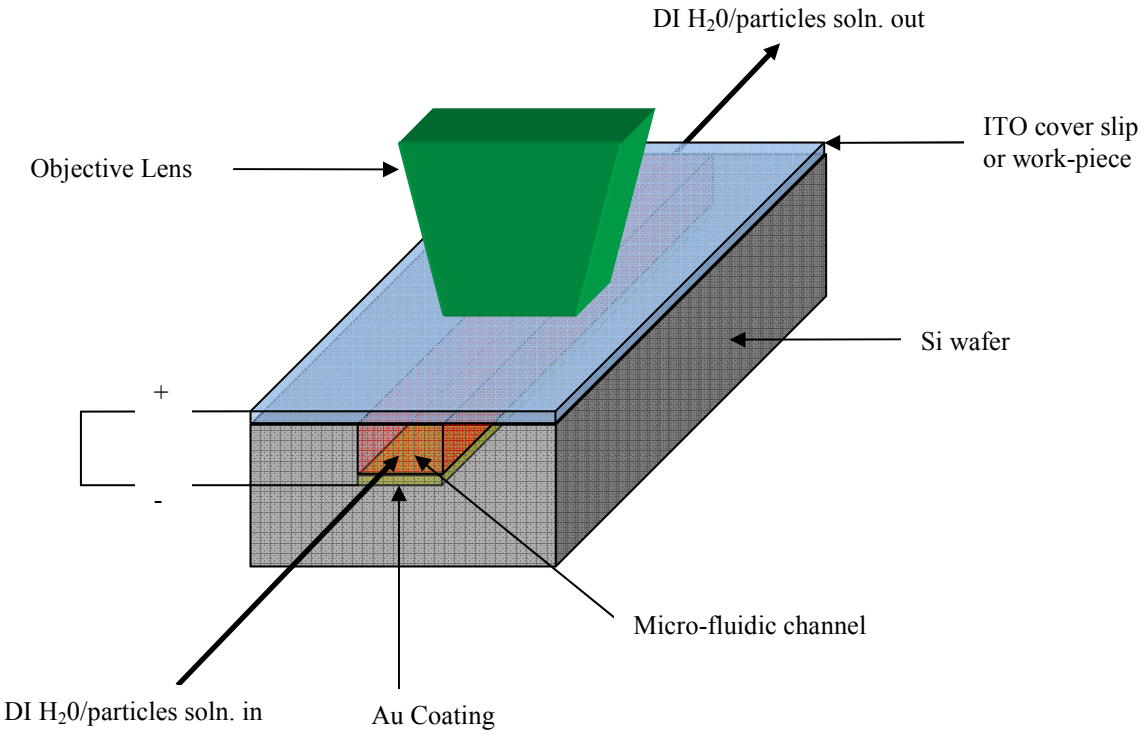

Figure 2. Design concept for micro-fluidic device

The MEMS device uses a silicon wafer base containing an etched micro-fluidic channel. Gold has to be deposited at the base of the channel in order to create an electrode. The silicon wafer has through-holes etched at the ends of the channel to allow for fluid to be

pumped in one end of the channel and exit out the other (not seen in Figure 2). The base silicon wafer is covered with an ITO coated glass cover slip through which the particles in motion may be viewed with a microscope. The ITO is the second conductive electrode to which a potential may be applied vertically between the two substrates. The glass cover slip is clamped to the silicon plate to prevent any fluid from leaking out of the channel. In order to select the most effective process for creating channels on a wafer the device needed the following characteristics; Fluid leakage out of the channel during fluid flow is minimized, gold must be absent from the walls of the micro-fluidic channel so that only a vertical electric field should exist to manipulate particle motion, and areas had to be allotted on each substrate to solder leads onto without the leads interfering with fluid motion or sealing between the two substrates. For example, it is obvious that a lead cannot be soldered onto the gold at the bottom of the channel because that would affect the fluid flow and make it extremely difficult to create a tight seal between the two substrates with a wire causing an obstruction. Preventing fluid leakage was essential because a loss of solution out of the channel decreases the number of particles that will interact with the surface in wear experiments.

3.1 Mask Design

Photolitography was used to create channels in the silicon wafer. The process involved creating a mask with multiple channels of the same dimensions and dicing the wafer into equally sized substrates. The length and width of the substrates was based on the size of the ITO coated cover slips. The cover slips were procured from SPI Supplies® with a resistivity of 8-12 ohms and measure 22 x 40 mm with a thickness between 0.16 and 0.19 mm.

The plan at the beginning of research on this project was to visualize how particle motion was affected by different channel dimensions. Therefore, originally three separate masks were designed with various channel depths and widths. Four channels were created on each mask with four equivalent substrate dimensions. However, using various dimensions for the channel proved troublesome because an extra variable influencing particle motion was introduced. Instead, channel dimensions were kept constant and only one mask was required for creating the channels. The channel measured 0.3 mm wide and 30 mm long, with a depth of 0.4 mm. For each substrate to be diced, the dimensions were chosen to be 27 x 40 mm. Note that the length of the substrate is equal to that of the ITO cover slip but that the width of the substrate is 5 mm larger than the cover slip. This is due to the fact that 5 x 5 mm square section was designed onto the left side of the substrate in order to create an area for a wire to be soldered to it. A second negative mask was designed to create through-holes in the wafers which provide reservoirs for fluid to enter and exit the channel. These through-holes measured 2 mm in diameter and were located flush with both ends of a channel. Figure 3 illustrates the two designs used to create the micro-fluidic channels and through-holes reservoirs.

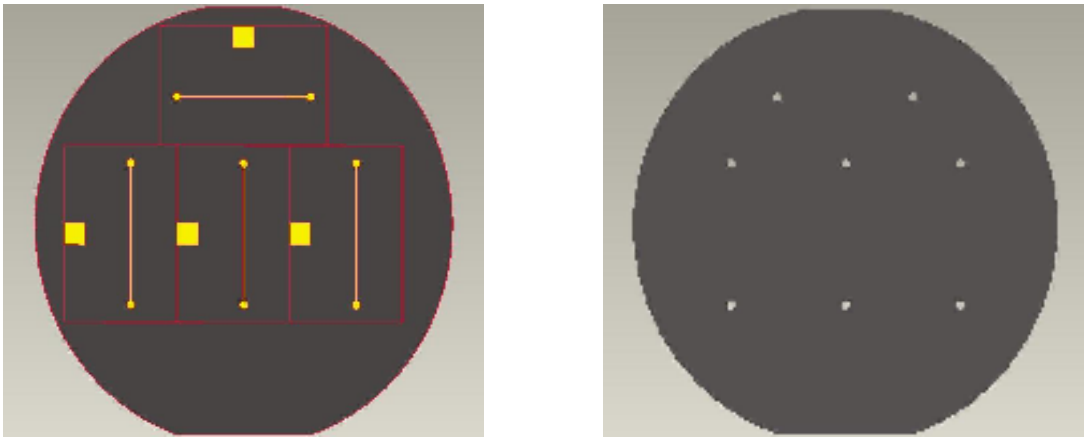

Figure 3. Two masks used to create channels and through-holes in 101.6 mm silicon

3.2 Substrate Preparation and Photolitography Process

Photolitography was used to create the surface features of the base substrate. This process is highlighted in Figure 4. The lithography process was performed on 101.6 mm N-type single side polished silicon wafers. The wafers were first oxidized to form a 1μm layer of silicon dioxide (SiO_2). The SiO_2 provides a barrier layer which prevents electric charge penetration into the silicon wafer after application of an electric field. A layer of gold was then coated onto the layer of SiO_2 using a Magnetron sputter system. The Magnetron sputter system uniformly deposits films of material onto a substrate. The process is done in an evacuated chamber at relatively low pressure. The sputter guns are controlled by a radio frequency or DC power supply.

The Au layer had to be sufficiently thick to ensure that no breakdown occurred due to the electro-kinetic process. Chen et al. [15] reported that conductivity increases rapidly with film thicknesses approaching 100 nm and decreases for thicknesses between 100-200 nm with a max conductivity occurring at 100 nm. Therefore, an Au film thickness of 100 μm was chosen. Photo-resist was then patterned on top of the gold layer to form the channel structures. Backside alignment and exposure of resist was performed on a Karl Suss mask aligner and deep reactive ion etching (DRIE) was employed to create the through-hole reservoirs at the ends of each channel. Polydimethylsiloxane (PDMS) was applied onto the wafer and cured. The PDMS was cured for three hours under vacuum at approximately 30 in Hg at a temperature of 90^{o}C. PDMS was chosen as the material to form channels because its adhesive properties provided a tight seal between the base substrate and ITO coated cover-slip or metal coated work-piece. After

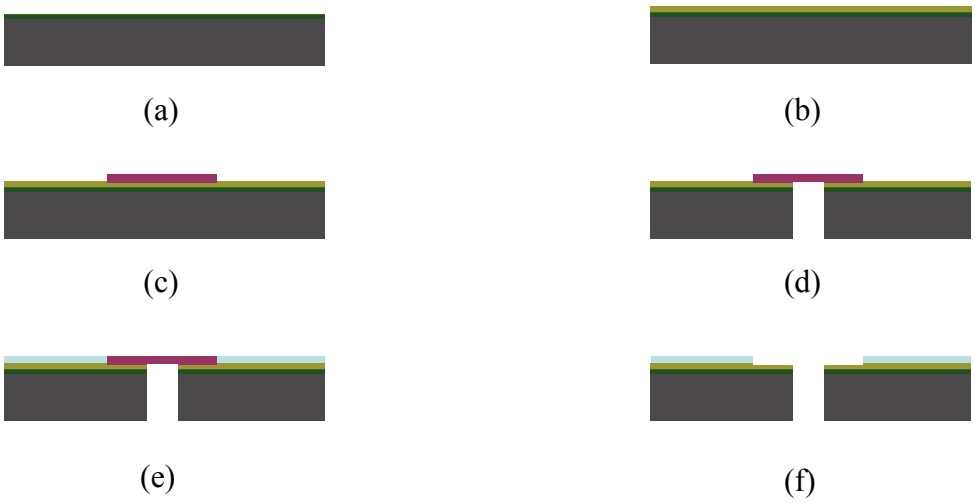

Figure 4. Photolitography process used to create base substrate including (a) deposition of 1µm SiO_2 (b) sputtering 100 nm Au (c) application of resist (d) DRIE to create through-hole reservoirs (e) application and curing of PDMS (f) RIE removing resist to form channels.

curing the PDMS, reactive ionic etching was employed to remove the PDMS to form the channel structures.

The wafers were developed and diced to create four equally sized base substrates per wafer. Dicing was done on a DISCO DAD 341 automatic wafer dicing machine using fine blade 35HEEE cutting fluid. The final step of fabrication for the base substrate was to connect two NanoPort^{TM} fluid connectors to the backside of the substrate centered over the two reservoirs at the end of the micro-fluidic channel. The connectors allowed for solution to be pumped into one reservoir, flow through the channel, and exit out of the other reservoir. Double-sided adhesive rings were placed around both reservoirs and onto the connectors themselves and the connectors were attached and cured at 121 ^{o}C for 95 minutes. This completed the process of preparing the base substrate.

A set of top substrates which served as the work-piece for the wear experiments also were fabricated. The selections of metal materials deposited onto the wafer were

carefully considered when preparing the work-piece substrates. The main requirements for the material were that it should be inert as well as able to easily deposit onto the substrate. It was also important to use at least two different metal material layers to prove that multiple layers can be eroded by the same process. The two metals chosen as the coatings for the work-pieces were copper and gold. 1 μm of SiO_2 were first grown onto each wafer to prevent electric charge from leaking into the silicon. A 1μm layer of Cu was then spin coated onto the layer of SiO_2 followed by a 100 nm layer of Au. Each coated wafer was diced into four equally sized pieces measuring 27 x 40 mm which is equivalent to the dimensions of the base substrate.

3.3 Clamp Design

A clamp was designed in order to create a tight seal between the base substrate with both the ITO coated cover-slips for visualization experiments and the metal coated work-piece for wear experiments. The clamp consisted of two machined aluminum plates, depicted in Figure 5.

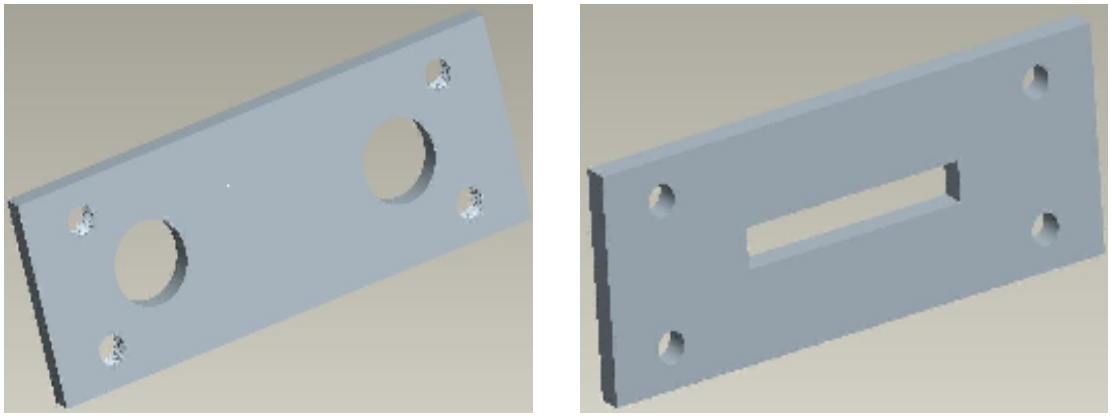

(a) (b)

Figure 5. A Pro-Engineer drawing of the clamping mechanism which includes (a) a base plate and (b) a top plate

Both the base plate and top plate of the clamp were 22 mm wide and 60 mm long with the base plate and top plate measuring 4 mm and 3 mm thick, respectively. The width of the plates were designed to be 5 mm shorter than the width of substrates which allowed the edge of the base substrate to hang outside of the clamp so that a wire could be soldered to the 5 x 5 mm square section of exposed Au. The length of plates were designed to be 20 mm longer than the length of the substrates allowing for screw holes to be machined into the four corners of the plates. Two 9 mm holes were machined into the base plate to allow for the Nanoport^{TM} connectors on the backside of the base substrate to stick through the plate which allowed for tubing to be connected between the connectors and the syringe pump. Four 3.5 mm threaded holes were also machined into the corners of the base plate. The top plate was designed to have a 4 x 26 mm window machined out of the center of the aluminum so particle motion in the micro-fluidic channel could be observed under an inverted microscope. Four screw holes measuring 3.2 mm in diameter were machined in the four corners of the top plate allowing for the screws to be inserted into the clamp. With a clamping mechanism in place, the entire device was then ready to be assembled.

3.4 Device Assembly

The final stage of constructing the micro-fluidic device was to solder leads to the base substrate, ITO coated cover-slip, and metal coated work-piece. After soldering was completed, the device was clamped together and prepared for experimentation. Figure 6 is a representative side and top view of the constructed device. Note that soldered wires are not represented in this diagram. The base substrate was placed on top of the base plate of the clamp with the channel facing up and the connectors going through the

allotted holes on the base plate. For visualization experiments, an ITO coated cover-slip was placed on top of the base substrate with the ITO coated side facing down. The cover-slip was slightly staggered in order for the soldered wire to hang off the edge of the

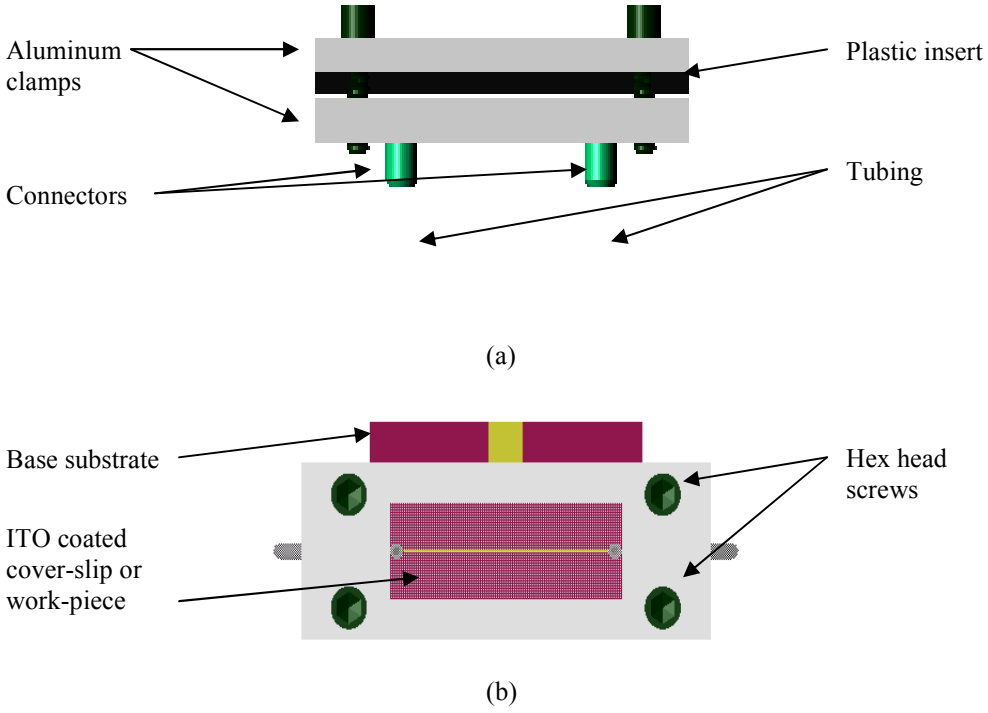

Figure 6. Assembled micro-fluidic device with (a) representing the side view and (b) representing the top view. Designed and constructed at Nanyang Technological University.

clamp as to not interfere with the seal. For wear experiments, the metal coated work-piece was placed on top of the base substrate with the metal coated side facing down. The work-piece was also staggered so that a wire soldered to the top gold layer would not interfere with the seal. A plastic insert was placed around the edges of the bottom of the top plate of the clamp creating a stronger seal between the substrate and the cover-slip or work-piece.

Hex head screws were used to tighten the device together. It is important to note the clamping procedure was very carefully executed as to not crack the wafer pieces and cover-slips by over tightening. Finally, tubing was attached to the connectors and the device was ready for experimentation.

Chapter 4: Experimental Setup

4.1 Experimental Variables

Once the micro-fluidic device was constructed, particle visualization and abrasive wear experiments were designed and conducted. Before these experiments could be executed, a set of experimental variables were defined. These experimental input variables are listed below in order of importance:

- AC Voltage/Electric Field Intensity
- Fluid flow rate
- Signal frequency
- DC coupling
- Particle size and type
- Solution concentration

The most important variable was the AC voltage because the primary concern of this thesis was to determine how various field intensities affected the wear rate of the metal work-piece. The magnitude of the AC voltage was the only parameter varied during the course of experimentation. Voltages were incremented by 5 Vpp over a range of 0-40 Vpp for this project. The solution was pumped into the channel at a rate controlled by a digital syringe pump. A flow rate of 0.25 μL/min was chosen so that particles were given sufficient time to reach the work-piece and remove material before the solution exited the channel. A frequency for the AC signal also had to be specified. At high frequencies, it was expected that more particles would approach the surface of the work-piece at a higher pace. However, Fagan *et al* [16] used a similar experimental setup to the one used in this thesis and reported that the height levitation of particles decreased with

frequencies increased past 100 Hz. Therefore, the frequency of the AC electric field was chosen to be 100 Hz. A positive DC bias was applied to the AC signal to force particles closer to the work-piece surface. The DC voltage was chosen based on particle visualization underneath the microscope. A bias of 5V was chosen because this was the highest possible DC bias that could be applied without creating cavitation. It was desirable to limit cavitation effects because the formation of bubbles in the micro-channel block fluid flow and hinder particles from reaching the work-piece surface. If fluid flow and particles are blocked by bubbles, material removal rates could be significantly lowered. Li and Cheng [17] reported that micro-channel size, mass flow rate, and heat flux play important roles in cavitation formation in liquid. The study concluded that large contact angles between the fluid and the substrate can effectively lower the nucleation temperature in a micro-channel. Also, higher mass flow rates tend to suppress bubble formation in a micro-channel. Lastly, the study concluded that axial heat conduction in the substrate may play an important role in the heat transfer process leading to cavitation formation. These factors effecting cavitation were important in designing the micro-fluidic device and for defining the experimental parameters. Because a rectangular micro-channel was used, it was realized that corners in the micro-channel were areas susceptible to cavitation formation. Also, since a low mass flow rate was used electric field strengths had to be lower than if higher mass flow rates were used.

Particle type and size were also specified. The sizes and zeta potentials of the particles in DI solution were measured using a Malvern™ Instrument Zeta-sizer nano ZS. Fluorescent spherical polystyrene (PS) particles measuring 0.964 μm in average diameter with an average zeta potential of

-69.88 mV were used for particle visualization experiments. Abrasive spherical silica particles were chosen for wear experiments because their electrical properties were similar to those of the PS beads. The silica particles measured 1.034 μm in diameter with a zeta potential of -54.8 mV. Table 1 lists the statistical analysis of the particles used for experimentation.

Table 1. Statistical analysis of the particles used for experimentation

	Average diameter (μm)	Diameter standard deviation (μm)	Average Zeta potential (mV)	Zeta potential standard deviation (mV)
Polystyrene particles (PS)	0.964	0.021	-69.88	2.70
Colloidal Silica Particles (SiO_2)	1.034	0.151	-54.80	0.67

The solvent used in all experiments was deionized (DI) water. A dilute PS colloidal solution of 99.5 % volume DI water and 0.5% volume PS was used for visualization experiments so individual particle motions could be examined. This concentration was realized through a trial and error approach. Fluorescent PS particle concentrations needed to be low in order to visualize individual particle movement in the micro-channel. Higher PS concentrations were originally used and lowered until individual particle motion could clearly be observed. A higher concentrated silica colloidal solution of 98.13% vol. DI Water and 1.87% vol. colloidal SiO_2 particles was used for wear experiments. Higher concentrations of particles were used in the wear experiments compared to the visualization experiments because more particle interaction with the work-piece surface was desirable for material removal. Also, the concentration of SiO_2 particles for wear experiments is comparable to SiO_2 concentrations used in conventional CMP techniques.

4.2 Apparatus Setup

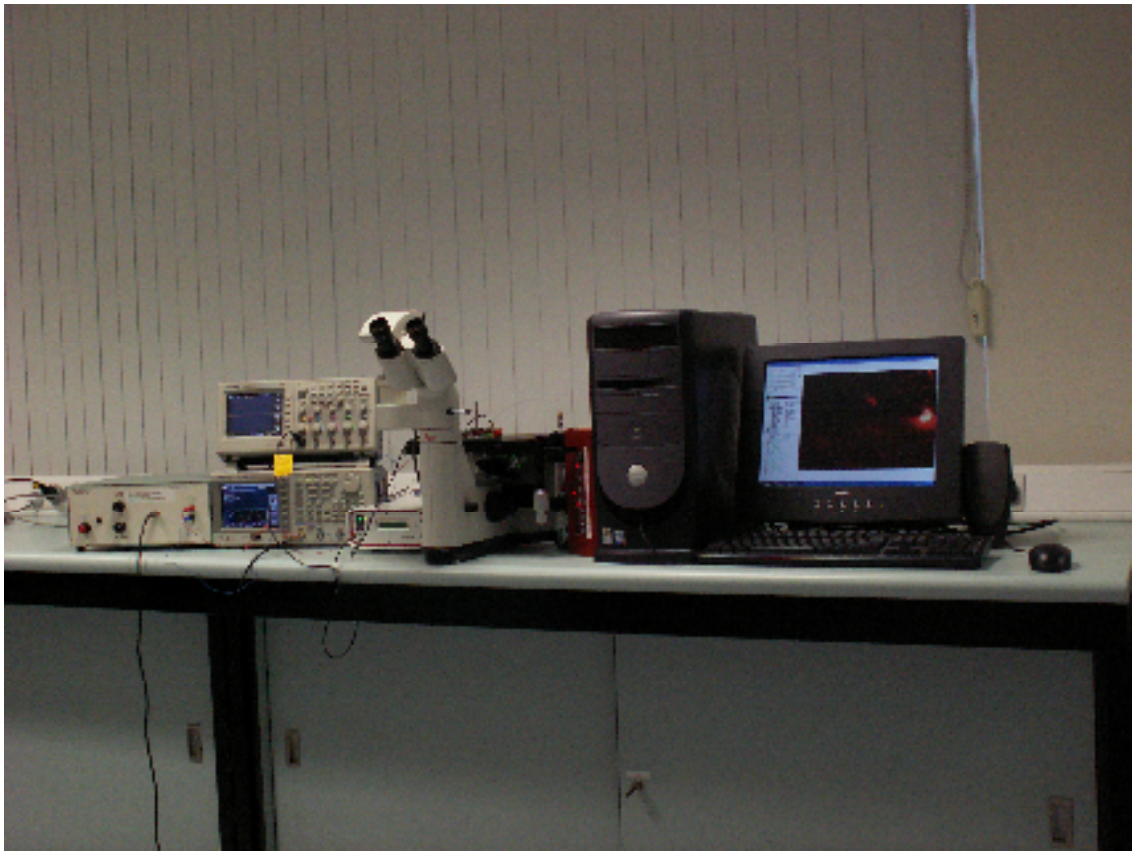

Figure 7. Photograph of the experimental setup for visualization and wear experiments containing voltage amplifier, function generator, oscilloscope, and inverted microscope with CCD camera, syringe pump, and computer.

Figure 7 shows a photograph of the experimental setup for performing both the visualization and wear experiments. For visualization experiments, the micro-fluidic device was placed cover-slip down onto the platform of a LEICA DMILM inverted micro-scope in order to observe particle motion. This was not required for wear experiments because the non-fluorescent silica particles could not be seen underneath the microscope. A NE-1000 syringe pump manufactured by New Era Pump Systems was used to propel solution through the channel at a constant flow rate. A Tektronix AFG 3022 Function Generator was used to generate the AC and DC signal. Since voltages

exceeding the threshold of the function generator were required for experimentation, an EPA-102 Piezo Amplifier procured from Piezo Systems Inc. was used to amplify the output signal from the function generator. The positive lead was connected to the ITO for visualization experiments and to the metal work-piece for wear experiments and the negative lead was connected to the base substrate. The negatively charged particles defined this orientation because particle movement to the work-piece surface was required for material removal. A Tektronix TDS 2014B oscilloscope was used to monitor the signal during experimentation.

4.3 Design of Experiments

Particle visualization experiments were conducted to observe particle motion in the channel at varying field intensities. The PS solution was pumped into the channel using the syringe pump and particle reactions were observed through the microscope at various AC signals, DC biases, frequencies, and flow rates. Table 2 gives the values of these tested parameters.

Table 2. Varied parameters for particle visualization experiments

Input Parameter	**Values Tested**	**Incremental Step**
AC Signal	0-50 Vpp	1 Vpp
DC bias	0-10V	1 V
Frequency	0-100 Hz	10 Hz
Flow Rate	0-1 µL/min	0.1 µL/min
Solution Concentration	99.5% DI H_2O/0.5%PS	N/A

Note that every combination of these parameters was not tested and no physical data was acquired from the visualization experiments. The goal of these experiments was to gain a better understanding of how each parameter affected particle motion to determine reasonable values of the input parameters for wear experiments. In Section 3.1 it was stated that only the AC signal was varied during wear experiments to determine how differences in electric field influenced metal wear rate. All other parameter values were held constant and resulted from particle observations and previous literature review. These values were also stated in Section 3.1 but are highlighted once again in Table 3 for convenience.

Table 3. Input parameters for abrasive wear experiments

Input Parameter	**Values Tested**	**Incremental Step**
AC Signal	0-40 Vpp	5 Vpp
DC bias	5V	N/A
Frequency	100 Hz	N/A
Flow Rate	0.25 µL/min	N/A
Solution Concentration	98.13% DI H_2O/1.87%SiO_2	N/A
Particles per unit volume	1.4 E10 SiO_2 particles/ml	N/A

Abrasive wear experiments were conducted at the nine specified AC voltages. An experiment was run for each voltage over time frames of 15, 30, 45, and 60 minutes, resulting in four experiments per voltage. Experiments for each voltage were repeated five times yielding a total of 180 experiments. The experiments in each trial were

randomly conducted to reduce the possibility of systematic errors. Table 4 shows the experimental matrix used for the abrasive wear experiments.

Table 4. Experimental matrix for 180 abrasive wear experiments. Each number represents the order each experiment was conducted for each trial.

Trial 1									
	0 Vpp	**5 Vpp**	**10 Vpp**	**15 Vpp**	**20 Vpp**	**25 Vpp**	**30 Vpp**	**35 Vpp**	**40 Vpp**
15 min	10	8	23	4	22	2	35	14	27
30 min	17	32	33	18	11	19	6	28	13
45 min	31	24	5	34	29	25	36	20	12
60 min	9	21	30	15	16	1	3	26	7
Trial 2									
	0 Vpp	**5 Vpp**	**10 Vpp**	**15 Vpp**	**20 Vpp**	**25 Vpp**	**30 Vpp**	**35 Vpp**	**40 Vpp**
15 min	20	18	11	32	22	9	7	12	5
30 min	25	34	33	16	15	28	14	23	35
45 min	19	24	36	31	27	30	29	13	6
60 min	4	26	17	21	8	2	1	10	3
Trial 3									
	0 Vpp	**5 Vpp**	**10 Vpp**	**15 Vpp**	**20 Vpp**	**25 Vpp**	**30 Vpp**	**35 Vpp**	**40 Vpp**
15 min	12	28	30	18	14	21	10	5	22
30 min	24	23	11	26	25	15	32	16	4
45 min	35	3	29	34	2	36	8	33	27
60 min	7	31	19	13	20	1	6	9	17
Trial 4									
	0 Vpp	**5 Vpp**	**10 Vpp**	**15 Vpp**	**20 Vpp**	**25 Vpp**	**30 Vpp**	**35 Vpp**	**40 Vpp**
15 min	24	4	16	10	6	32	2	20	8
30 min	29	31	26	28	23	13	19	14	22
45 min	11	5	35	1	34	36	33	27	3
60 min	17	30	12	25	15	9	18	7	21
Trial 5									
	0 Vpp	**5 Vpp**	**10 Vpp**	**15 Vpp**	**20 Vpp**	**25 Vpp**	**30 Vpp**	**35 Vpp**	**40 Vpp**
15 min	6	8	4	16	25	13	30	2	24
30 min	18	22	27	32	9	35	10	19	11
45 min	28	17	33	14	31	20	34	36	29
60 min	5	7	21	26	15	1	23	12	3

One metal coated work-piece was used for each column underneath each trial in Table 4. Each work-piece was slightly staggered to the side before an additional experiment was conducted, so that a separate trench was created in the metal for the given time periods. Figure 8 shows a schematic of three metal coated work-pieces with wear trenches for

each timed experiment used in Trial 2 of material removal experiments. After all four experiments were run on each work-piece, five surface scans per trench were taken using a Taylor Hobson Precision Talyscan 150 surface profilometer in order to determine the material removal rate. The five surface scans were taken at locations ranging from the beginning to the end of the trench. The scan locations were held as constant as possible for each work-piece. Upon completion of the experiments, all surface scans per trench which displayed material removal were averaged which yielded an average step height change per trench.

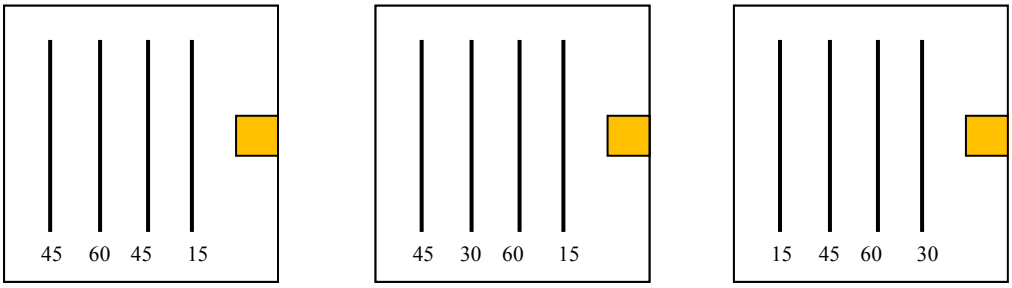

Figure 8. Schematic of work-pieces used in Trial 2 for 5, 10, 15 Vpp, respectively. The numbers underneath each trench corresponds to a time period in minutes.

Table 5 lists a set of control experiments that were conducted so that additional insight into the removal mechanism could be obtained. These experiments were run to determine if there are other mechanisms other than mechanical material removal present. Surface scans were also performed on the work-pieces used for the control experiments to determine material removal rates, if present.

Table 5. Abrasive wear control experiments

Experiment	DI H_2O Vol [ ] (%)	SiO_2 Solution Vol [ ] %	AC Voltage (Vpp)	DC bias (V)	Flow Rate (µL/min)	Frequency (Hz)
1	100	0	25	5	0.25	100
2	100	0	0	0	0.25	0
3	98.13	1.87	25	5	0	100
4	98.13	1.87	0	0	0.25	0
5	98.13	1.87	0	5	0.25	0

Chapter 5: Mathematical Model

In order to determine how to properly model material removal using the electro-kinetic approach, the behavior of PS and silica particles under the influence of electric field had to be understood. This chapter presents the behavior of a particle in a micro-channel as well as the forces which act on the particle during the electro-kinetic process. Defining the particle behavior and force balance on a single particle allowed for a mathematical model of the metallic material removal to be realized.

5.1 Particle Behavior and Force Balance

As mentioned in the previous chapter, a syringe pump injects colloidal solution into the channel of the micro-fluidic device at a constant velocity and an electric field is induced to bring particles to the surface and oscillate against it. Figure 9 illustrates the particle motion in the micro-channel. Step 1 in the figure represents horizontal motion of the particle in the x-direction due to pressure driven flow. The particle moves in the horizontal direction until influenced by a positive DC bias in step 2. The DC bias raises the negatively charged particles to the positively charged top work-piece or ITO cover-slip. It was necessary for the DC bias to be implemented so that a greater percentage of particles were present at the work-piece to participate it material removal. Step 3 represents the response of the particle with the addition of the AC signal to the DC bias. The particles repeatedly collide with the work-piece and thus participate in metallic material removal.

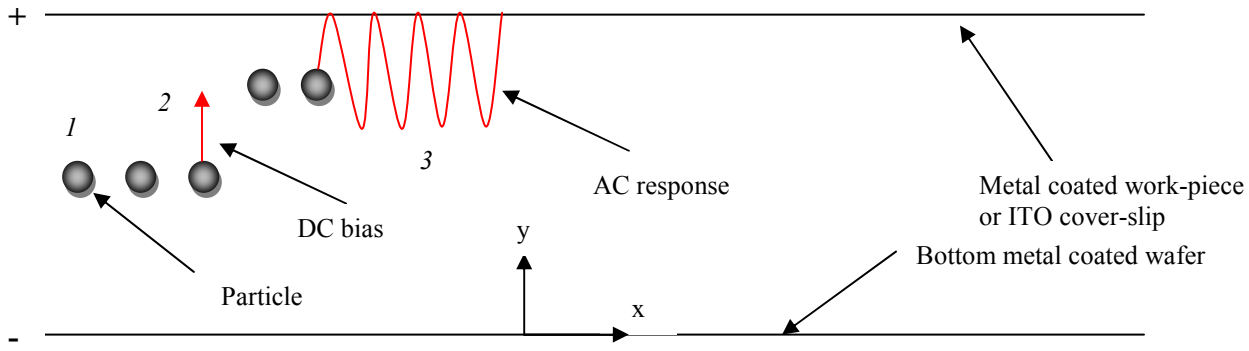

Figure 9. Particle motion in micro-channel resulting from pressure driven flow, DC biasing, and an AC signal

There are a number of forces that act on an abrasive particle in a colloidal solution moving through a micro-channel. Forces act in both the x and y direction, however, the primary focus was to determine the net force acting in the y-direction in order to determine the pressure exerted on the work-piece by an abrasive particle. Before the forces are defined, it is important to state the assumptions governing the force balance. These assumptions are listed below:

1. The electric field is uniform, acting only in the y-direction. Therefore, the particle would experience no dielectrophoretic force due to the electric field. The force due to the electric field is simply an electrostatic force.
2. Fluid flow is steady state at a low Reynolds number. Reynolds number is given by:

$$Re = \frac{\rho v d_c}{\eta} \tag{5.1}$$

where ρ, v, and η are the fluid density, velocity, and kinematic viscosity, respectively, and d_c is the channel depth. The Reynolds number for fluid flow in experimentation is 0.031 which is safely in the range for laminar flow. Therefore, the colloids move at the same velocity as the fluid.

3. Forces can be described as acting on the center of the particle although these act on the surface. This allows the equation of motion on the cell to be simplified without losing generality.

The main forces that are acting on the particle in are the pumping force F_{pump}, the electrostatic force F_E, the natural forces F_N, and the drag force F_{drag}. Figure 10 is a free body diagram of the forces acting on the particle. Since this situation represents a low Reynolds number, steady state flow has been assumed so that there is no need to complete the force balance in the x-direction. It is reasonable to assume that the colloidal particles are moving at the same velocity as the solution since acceleration is equal to zero. As mentioned earlier, the solution was pumped into the channel at a constant volumetric flow rate, Q. The fluid flow rate was converted into the fluid velocity using the following equation:

$$V_{fluid} = \frac{Q}{A_c} = \frac{Q}{d_c w_c} \tag{5.2}$$

where A_c is the area of the channel and d_c and w_c are the channel depth and width, respectively. As a result of the fluid flow assumptions, it can be stated that

$v_{fluid} = v_{part\_x}$.

The forces acting on the particle in the y-direction are the electrostatic force, F_E, the normal forces, F_N, and the drag force, F_{drag_y}. The force balance in the y direction is written as

$$F_E - F_N - F_{drag\_y} = m\frac{dv_y}{dt} \tag{5.3}$$

where v_y is the velocity of the particle at a certain position and time.

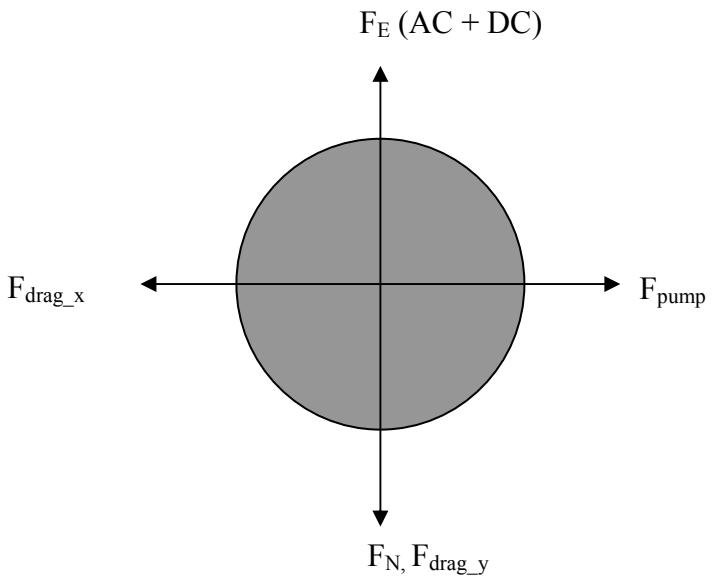

Figure 10. Free body diagram of the forces acting on a particle during the electo-kinetic process.

The mass of the particle is given by

$$m = \frac{\rho}{V} \tag{5.4}$$

where ρ is the density of the spherical particle and the volume is

$$V = \frac{4}{3}\pi a^3 \tag{5.5}$$

with *a* being the radius of the particle.

The electrostatic force [14] exerted on a particle by an applied electric field is given by

$$F_E = 4\pi a \varepsilon_r \varepsilon_o \varsigma E f(\kappa a) \tag{5.6}$$

where ε_r is the permittivity of the DI H_2O medium, ε_o is the permittivity of a vacuum, and ζ is the measured zeta potential of the particle. The equation for the applied electric field is written as

$$E = E_{AC} + E_{DC} \tag{5.7}$$

where E_{AC} and E_{DC} are the alternating and direct current components of the electric field, respectively. The AC component of the electric field is given by

$$E_{AC} = \frac{A\sin(\omega t)}{kd_c} \tag{5.8}$$

where A is the amplitude of the AC signal, ω is the frequency, t is time, k is the dielectric constant of the medium, and d_c is the channel depth. The DC component of the electric field is given by

$$E_{DC} = \frac{V_{DC\_Bias}}{kd_c} \tag{5.9}$$

where V_{DC_bias} is the amplitude of the applied DC bias. Henry's function, $f(\kappa a)$, relates the particle's zeta potential to its electrophoretic mobility and is written as

$$f(\kappa a) = 1 + \frac{1}{2[1 + \frac{2.5}{\kappa a(1 + 2e^{-\kappa a})}]^3} \tag{5.10}$$

where e is the fundamental unit of charge and κ is the Debye parameter given by

$$\kappa = \sqrt{\frac{2e^2 z^2 n_o}{\varepsilon_r \varepsilon_o k_b T}} \tag{5.11}$$

where z is the valence on the particles in at the symmetric electrolyte, n_o is the ionic concentration in bulk solution, k_b is the Boltzmann constant, and T is the temperature of the solution.

The natural forces on a colloidal particle include its weight and the buoyancy force. The equation for the natural force on a particle is given by Stokes drag equation

$$F_N = 3\pi\eta d\frac{dy}{dt} \tag{5.12}$$

where η is the viscosity of the medium, and d is the diameter of particle.

An additional force acting in the y-direction is the drag which resists the movement of the particle in the DI H_2O medium. The drag equation is given by

$$F_{drag\_y} = 6\pi\eta a \frac{dy}{dt} \tag{5.13}$$

Substituting equations 5.6-5.13 into equation 5.3 yields the complete force balance equation in the y direction

$$4\pi a\varepsilon_r\varepsilon_o\varsigma[(\frac{A\sin(\omega t)}{kd}) + (\frac{V_{DC\_Bias}}{kd})]f(\kappa a) - \frac{[d^2(\rho_s - \rho_w)g]}{18}3\pi d - 6\pi a\eta(\frac{dy}{dt}) = m\frac{d^2y}{dt^2} \tag{5.14}$$

The dominant force in the electro-kinetic process is the electrostatic force. However, the drag force and the normal forces acting on the particles have a small effect. Therefore, a close approximation of the net force acting on a particle in the y-direction is

$$F_{net\_y} \approx F_E - F_N - F_{drag\_y} \tag{5.15}$$

5.2 Material Removal Model

Once the net force in the vertical direction, $F_{net\_y,}$ was determined, the model governing material removal was analyzed. Figure 11 depicts the mechanism leading to metallic material removal from the work-piece surface.

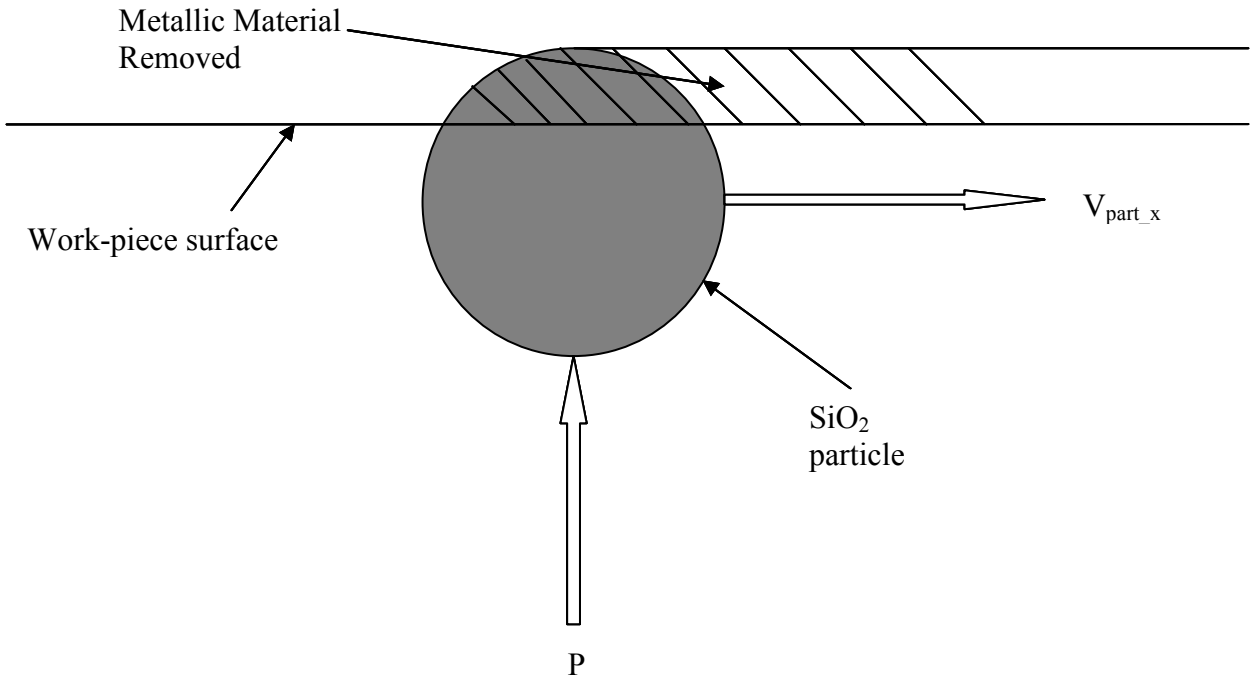

Figure 11. Mechanism governing metallic material removal from work-piece surface

During the electro-kinetic material removal process, each individual SiO_2 particle exerts a net force in the y-direction nearly perpendicular to the work-piece surface. As a particle makes contact with the work-piece surface, a pressure is exerted on a very small circular contact area on the surface. The horizontal velocity of the particle then slightly drags it across the surface removing a small portion of the metallic surface material before the particle is forced away from the surface by the negative portion of the AC signal.

The mechanism for material removal by the electo-kinetic phenomena is analogous to the CMP process. The Preston equation [18] was derived from observation of glass polishing processes and was adopted as the standard for modeling CMP. The equation predicts that material removal rate is proportional to pressure applied and pad velocity

$$Material\ Removal\ Rate = k_p\ x\ Pressure\ x\ Velocity$$

where k_p is the Preston constant that could be a function of all other input variables in the process.

Electro-kinetic metallic material removal is a mechanical process which is similar to mechanical abrasion models presented for CMP. Luo et al. [19], Zhao et al. [20], and Ng [21] proposed that abrasive particles caught between the tips of the asperities in a polishing pad and the silicon wafer were responsible for material removal from the wafer. Luo modeled the abrasive-wafer and abrasive-pad-solid-solid contacts as plastic contact between wafer and abrasives. Zhao's approach was a bit different as he modeled elastic contact between the pad and abrasives, and plastic contact between the wafer and abrasives. Both models predicted mean material removal from the wafer surface.

The model presented for the electro-kinetic process is based on mechanical abrasion using Preston's equation and Hertzian analysis to determine the contact area and pressure exerted by a SiO_2 particle on the work-piece surface. Hertz [22] postulated two solids coming into contact under a normal load will have normal displacements at the surface in a circular contact area. Given that the significant dimension of the contact area, a, and the relative radius of curvature, R, of the radii of each body R_1 and R_2, and

the significant dimensions of the bodies both laterally and in depth by l , Hertz made the following assumptions that govern Hertzian theory for elastic contact:

1. The surfaces are continuous and non-conforming: a<<R
2. The strains are small: a<<R
3. Each solid can be considered an elasitic half space: $a<<R_{1,2}$, a<<l
4. The surfaces are frictionless: $q_x=q_y=0$

These assumptions allow for the pressure distribution acting over a surface area of two elastic half-spaces to produce normal displacements in the two surfaces.

The maximum pressure in the distribution had to be found because the maximum pressure results in highest MRR at a given area of the work-piece surface. The highest MRR for the model is desired because the maximum depths of the surface scans for the experimental results were taken as experimental data. The peak Hertzian pressure is given by

$$P_o = (\frac{6F_{net_y}E^{*2}}{\pi^3 R^2})^{\frac{1}{3}} \tag{5.16}$$

where the contact radius $R=a$ because the particle comes into contact with a rigid flat work-piece. The effective Young's modulus is given by

$$E^* = (\left(\frac{1-\nu_{gold}^2}{E_{gold}}\right) + \left(\frac{1-\nu_{Silica}^2}{E_{silica}}\right))^{-1} \tag{5.17}$$

where v_{gold}, E_{gold}, v_{silica}, and E_{silica} are the Poisson's ratio and Young's modulus of the gold work-piece surface and the SiO_2 particles, respectively. Once the maximum pressure is calculated, the material removal rate is found by the following equation:

$$MRR = k_p V_{part\_x} P_o \tag{5.18}$$

This equation evaluates the maximum depth of material removal per time per SiO_2 particle in solution. The width of removal for a single particle is very small and a number

of particles colliding within a localized area cause the larger removal widths seen in the experimental results in the following chapter. Ng [21] reported a Preston's coefficient k_p= 4.70E-13 during the CMP process and this number was used to calculate model material removal rates for this thesis. Recall from equations 5.6-5.9, 5.15, and 5.16 that the material removal rate is directly proportional to electric field strength. Combining these equations yields:

$$MRR = k_p V_{part_x} \left(\frac{6\left(4a\varepsilon_r\varepsilon_o\zeta Ef(\kappa a) - 3v\eta d - 6\eta a\frac{dy}{dt}\right)E^{*2}}{\mu^2 R^2}\right)^{\frac{1}{3}} \quad (5.19)$$

The effect of electric field on the material removal rate is explained later in section 5.2. Table 6 lists the constants and their respected values used to solve the equations in the model.

Table 6. Constants and their respected values used to solve force balance equations.

Constant	Value	Units
Q	2.5 E-10	m^3/min
η	8.90 E^{-4}	kg/ms
d (SiO_2 particles)	1.034 E^{-6}	m
d (PS particles)	0.964 E^{-6}	m
ρ (SiO_2 particles)	2000	kg/m^3
ρ (PS particles)	1050	kg/m^3
ρ_w (DI H_2O medium)	1000	kg/m^3
ε_r	80	N/A
ε_o	8.854 E^{-12}	C^2/Nm^2
ζ (SiO_2 particles)	-69.88 E^{-3}	V
ζ (PS particles)	-54.87 E^{-3}	V
k	76.7	N/A
d_c	400 E^{-6}	m
w_c	300 E^{-6}	m
e	1.602 E^{-19}	C
z	1	N/A
n_o	6.023 E^{19}	N/A
k_b	1.381 E^{-23}	J/K
T	298	K
m (SiO_2 particles)	1.158 E^{-15}	kg
m (PS particles)	4.925 E^{-16}	kg
$v_{part\ x}$	3.47 E^{-5}	m/s
v_y (approximate)	1.3E^{-5}	m/s

Chapter 6: Results and Discussion

The results from the particle visualization experiments and material removal experiments are presented in this chapter. The visualization results were used to understand how the electric field affected particle motion and the material removal process. The metallic material removal results are compared to the mathematical material model and the discrepancies are discussed.

6.1 Particle Visualization Experiments

In chapter 3.3 the design of experiments was presented and the input parameters which were tested during visualization experiments were listed in Table 2. Fluorescent PS particles in solution were observed in the micro-channel of the device underneath the inverting microscope. The first experiment was to observe horizontal motion of the particles at various flow rates. A small amount of solution was pumped into the channel and allowed to settle without propelling the particles forward with pressure driven flow. The particles exhibited Brownian motion, moving around slightly with unpredictable motion. As the flow rate was incremented 0.1 μL/min over a range of 0-1 μL/min, the PS particles exhibited an expected increase in horizontal velocity. Each particle held its horizontal path through the channel unless it was struck by another particle, which slightly altered its trajectory.

The effect of DC biasing on particle motion was then tested by incrementing the DC bias by 1V over a range of 0-10 V. The horizontal flow rate was held constant at 0.5 μL/min and the AC Voltage was set to 0 Vpp. The positive DC bias caused the particles to move toward the top ITO cover-slip which served as the positive electrode. Increasing the DC bias caused a greater percentage of the particles to reach the surface of the cover-

slip. This observation was expected because the negatively charged particles are attracted to the positively charged surface. Higher positive potentials create higher magnitudes of forces that push the particles toward the surface. The DC bias also caused particles to align near the side walls of the channels. This was an unexpected observation but makes sense because the electric field lines bend toward the side channel walls, causing a highly concentrated potential in that area. The bias was switched from positive to negative to further prove the point that DC biasing brings particles toward the desired surface. This took the particles out of focus of the microscope which meant the negative bias forced particles away from the cover-slip surface. Once again, this was expected because the negatively charged cover-slip electrode repels the negatively charged PS beads. DC biases surpassing 5 V caused cavitation to form in the channel. Therefore, a 5 V DC bias was selected for material removal experiments. Figure 12 summarizes the study of DC bias on particle motion.

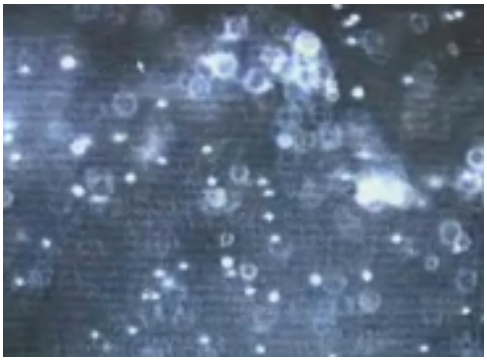

(a)

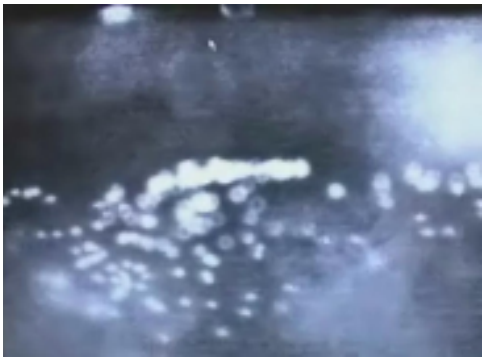

(b)

(c)

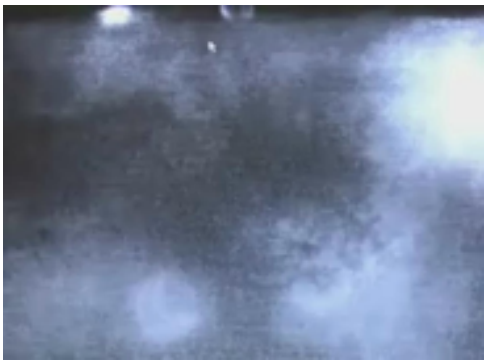

(d)

(e)

Figure 12. Summary of the effects of DC bias on PS particle motion (a) Particle dispersion at 0V DC bias (b) Particle movement transitioning from 0V to +5V DC bias (c) Particle alignment resulting from +5V DC bias for ~20 seconds (d) Particle positioning after DC bias switched from +5V to -5V for ~5 seconds (e) Cavitation due to AC voltage exceeding 25 Vpp and DC biases exceeding 5 V

Lastly, the effect of AC voltage on particle motion was examined by incrementing the AC voltage by 5Vpp over a range of 0-50 Vpp. Frequency effects were also observed by increasing the frequency by 10 Hz over a range of 0-100 Hz for each AC voltage. The horizontal flow rate was held constant at 0.5 μL/min and the DC bias was set to 0V.

The inverting microscope was focused on an area near the top cover-slip surface. Applying an AC signal caused the particles to "blink" because the particles were going in and out of focus. The "blinking" phenomena is the result of the AC signal cycling from positive to negative which changes the direction of the forces acting on the particle. Increasing the AC potential caused more violent particle "blinking". Increasing the AC frequency caused the particles the "blink" more rapidly. This is expected because a frequency increase produces more AC cycles per second. Cavitation began to form at 25 Vpp and became more significant at AC voltages exceeding 25 Vpp. This bubbling phenomenon raised uncertainty on the effect the AC voltages exceeding 25 Vpp would have on material removal experiments before the experiments were completed. The effect of cavitation on the material removal results will be more thoroughly discussed later in the chapter.

The particle visualization experiments provided insight on how the different parameters affect particle motion. This set of experiments led to the values selected in Table 3 for material removal experiments. The visualization experiments also supported the hypothesis for the mechanism of material removal, although a completely vertical uniform electric field was desired at the onset of the project. The material removal experimental results will provide further insight on how field lines bending to the side channel walls affect metallic wear.

6.2 Material Removal Experiments

The particle visualization experiments provided some valuable insight into the material removal process. The parameters tested in Table 2 provided the input parameters for the material removal experiments, listed in Table 3. Table 5 listed the control experiments that were completed to gain further insight into the material removal mechanism. Each of the control experiments was subjected to the process for 1 hour. Experiments 1 and 2 were run without SiO_2 particles in order to prove that abrasive particles in solution are necessary for metallic material removal. Zero wear was recorded for both experiments, which proved that SiO_2 particles were required to cause material removal. For experiment 3, solution was injected into the micro-channel and the electric field was induced but the solution was not propelled forward by a flow rate. Zero wear was recorded for this experiment, which proved that the particles required a horizontal velocity in order to remove material. Experiment 4 was completed with a horizontal flow rate, but no electric field. As expected, there was zero wear caused by the experiment which proved that an electric field must be present to induce wear. Lastly, experiment 5 was completed with a DC bias and horizontal flow rate, but no AC Voltage. Zero wear was recorded for this experiment which proved that both AC and DC electric fields must be present to remove metallic material from the work-piece surface.

The results presented no surprises about the mechanism for metallic material removal. Therefore, the experimental matrix laid out by Table 4 was completed to determine the effect of AC Voltage on metallic material removal. Figure 13 depicts area scan performed on all of the work-pieces in order to determine how material was being removed from the work-piece surface. Notice for each of the eight area scans

corresponding to each AC Voltage, material was removed in line segments across the width of the channel. These results were somewhat surprising due to the fact that uniform material removal across the width of the channel was desired. However, upon further evaluation the particle visualization results explained why material was being removed in the line segment fashion. Recall from section 5.1 that the DC bias caused particles to line up in the channel. Although Figure 12c showed only one line of particles, there were multiple lines present in the channel. These particle lines were present in approximately the same areas where material removal is shown on the work-piece surfaces in Figure 13. As the AC Voltage was increased the areas where material removal is present became darker which represents an increased penetration depth. These results were very encouraging because increased material removal was expected as AC Voltage was increased.

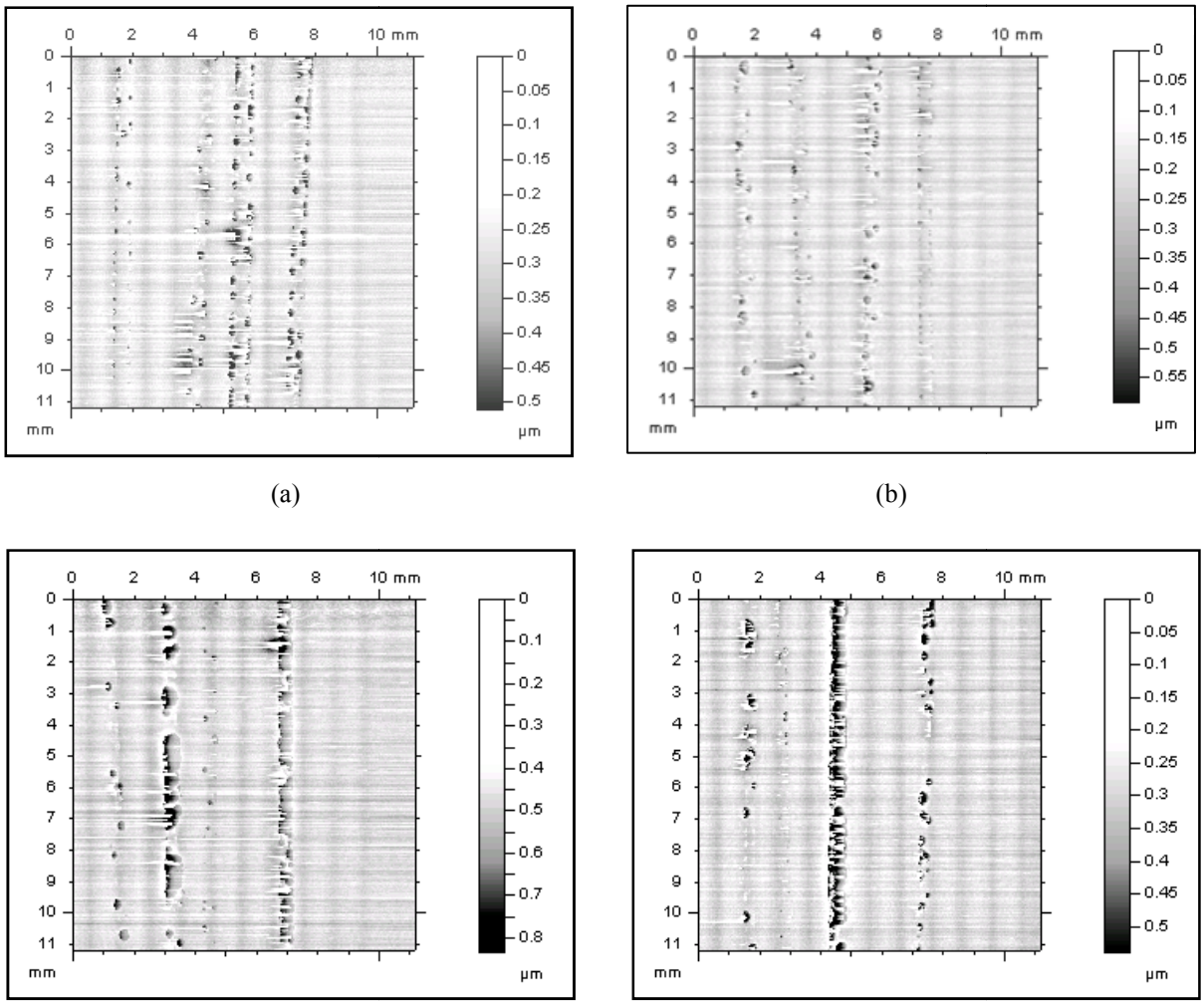

Figure 13. Area scans of metallic coated workpiece at a DC Bias of 5V and an AC Voltage of (a) 5 Vpp (b) 10 Vpp (c) 15 Vpp (d) 20 Vpp (e) 25 Vpp (f) 30 Vpp (g) 35 Vpp (h) 40 Vpp

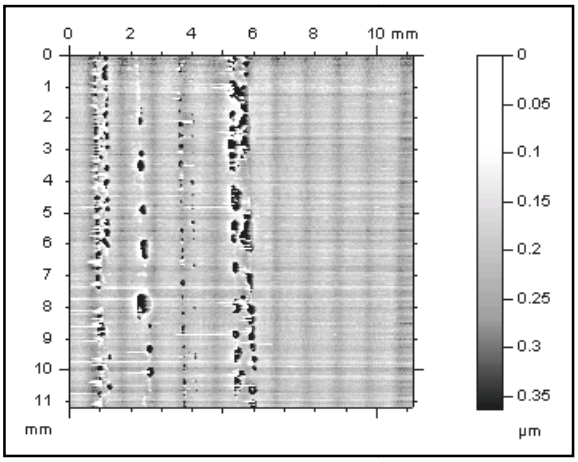

(e)

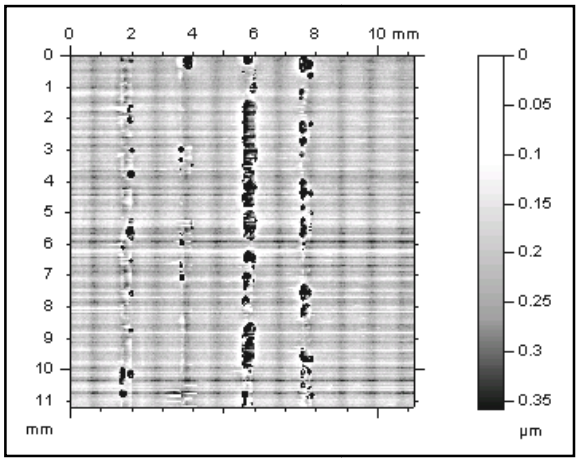

(f)

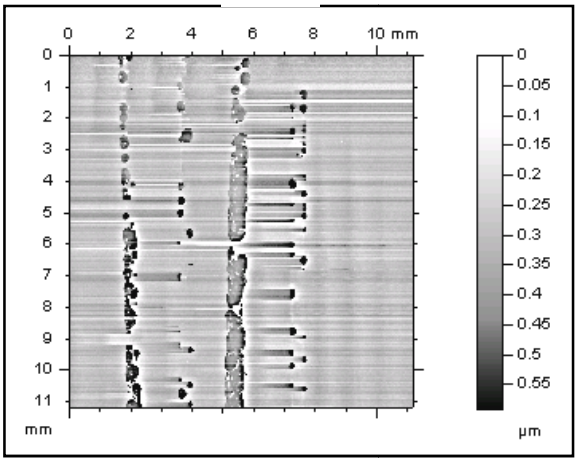

(g)

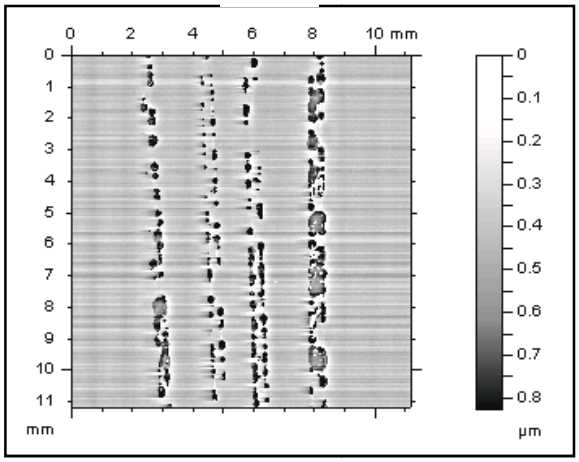

(h)

Figure 13 cont. Area scans of metallic coated workpiece at a DC Bias of 5V and an AC Voltage of (a) 5 Vpp (b) 10 Vpp (c) 15 Vpp (d) 20 Vpp (e) 25 Vpp (f) 30 Vpp (g) 35 Vpp (h) 40 Vpp

Line scans were also performed on the work-pieces in order to determine the wear depths creating by the electro-kinetic process. As mentioned in Section 3.3, five scans were taken of each trench created by the material removal process. Outliers representing wear data points which were excessively large compared to the rest of the data were removed. The remaining data was averaged yielding an average wear depth per AC voltage and time. These results are reported graphically in Figures 14-21.

Each figure represents average wear vs. time for a specified AC Voltage. Note that at time equal to zero, wear is equal to zero. The slopes of the three trend-lines on each graph represent a minimum, average, and maximum average material removal rate for each specified AC Voltage. Note that the minimum and maximum material removal rates acquired from the slopes in Figures 14-21 are average values as well because the five wear depths per trench were averaged together. Table 7 lists average, minimum, and maximum average material removal rates for each AC voltage. The general trend for each graph was an increase in material removal depth with increasing time. With increasing time, the areas of material removal were larger because the particles had more time to interact with the surface. As the areas of material removal grew, the larger the average wear depths became because the percentage of a line scan hitting a removal area was greater. Thus, the increasing average wear depth per time was an expected result.

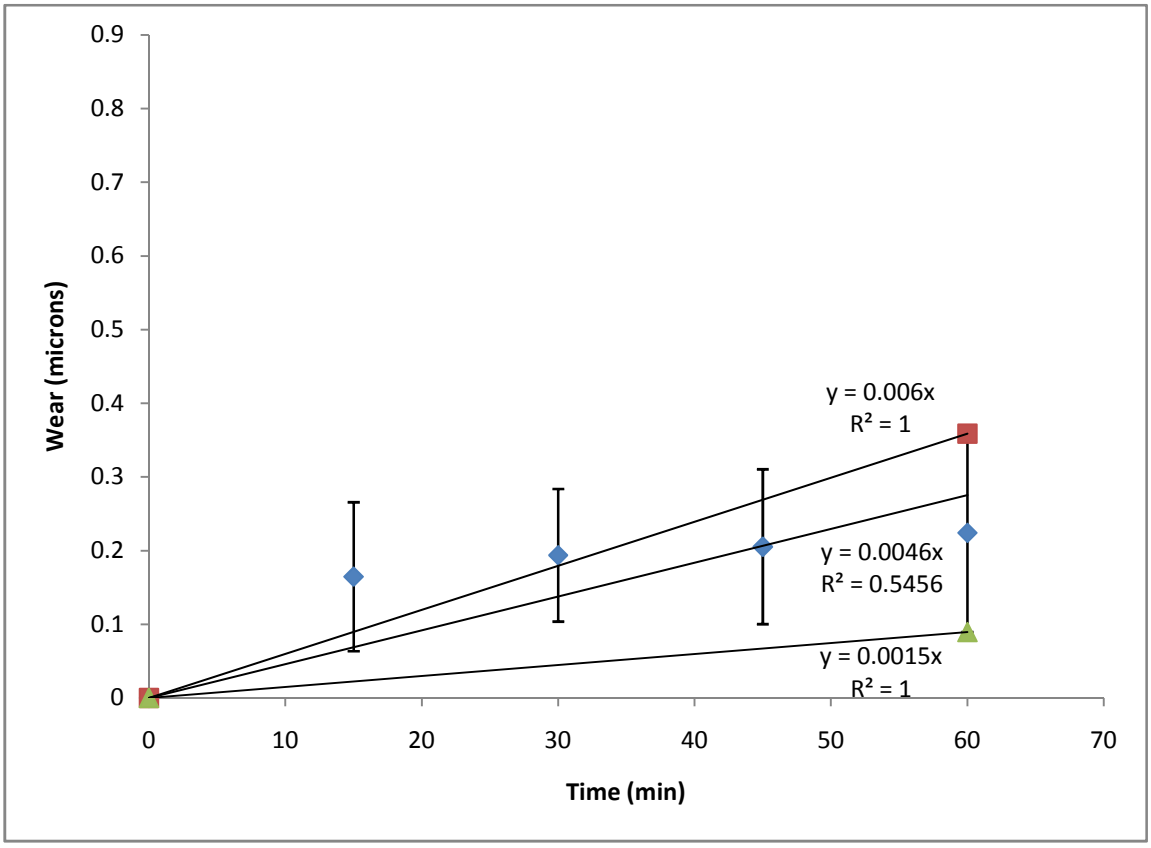

Figure 14. Metallic wear vs. time: 5 V DC, 5 Vpp

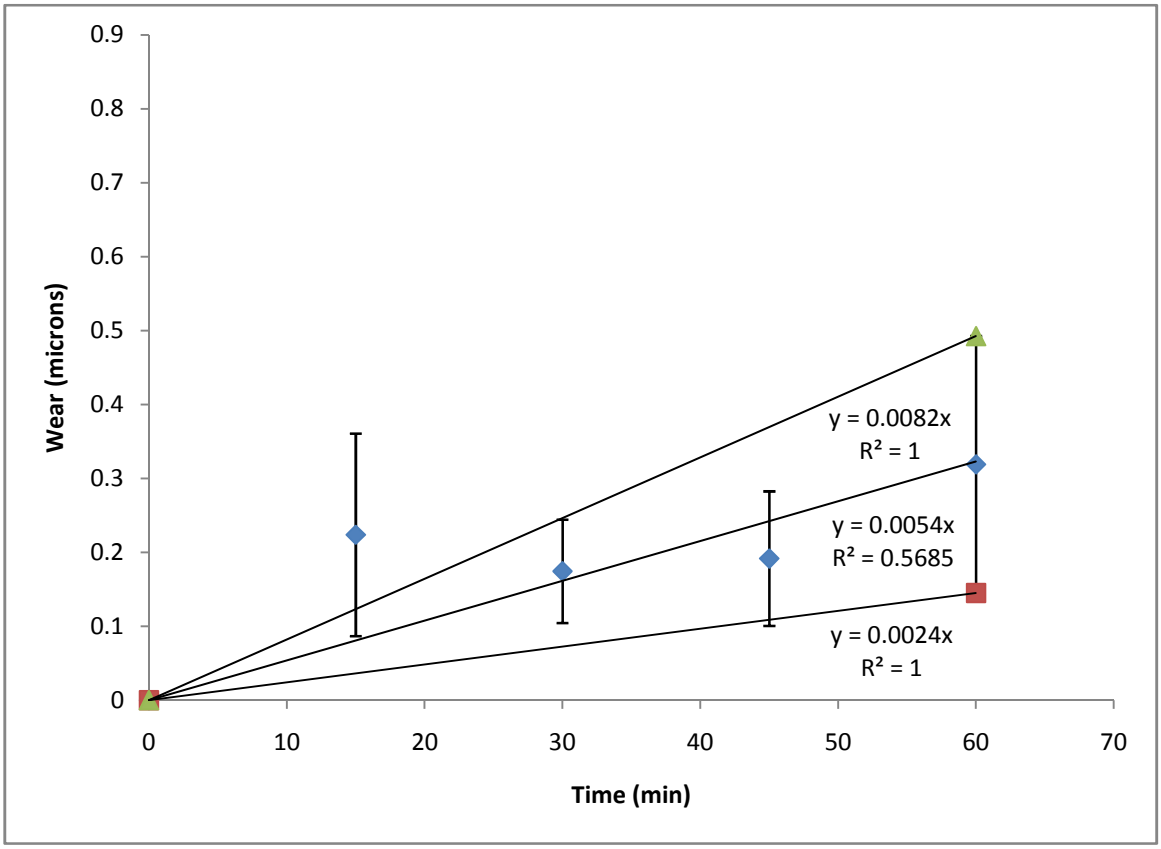

Figure 15. Metallic wear vs. time: 5 V DC, 10 Vpp

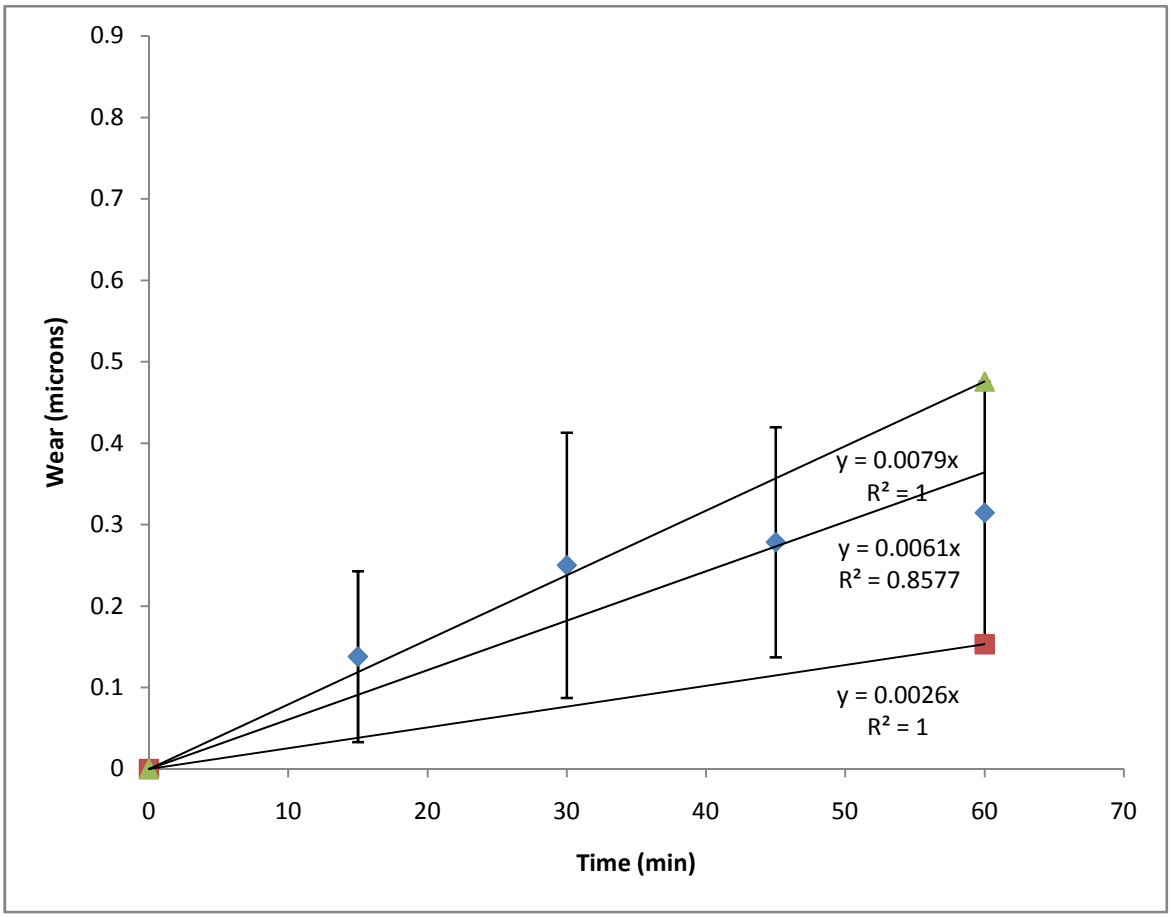

Figure 16. Metallic wear vs. time: 5 V DC, 15 Vpp

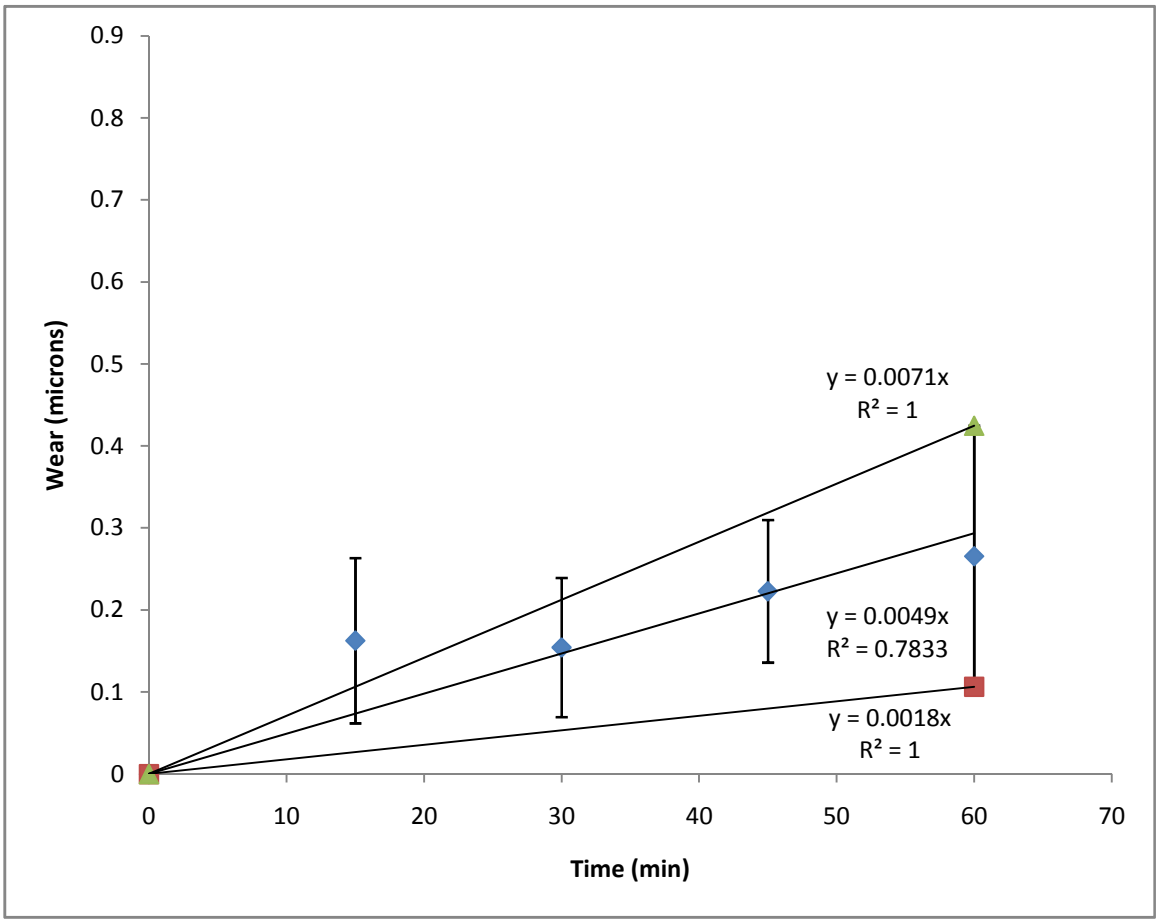

Figure 17. Metallic wear vs. time: 5 V DC, 20 Vpp

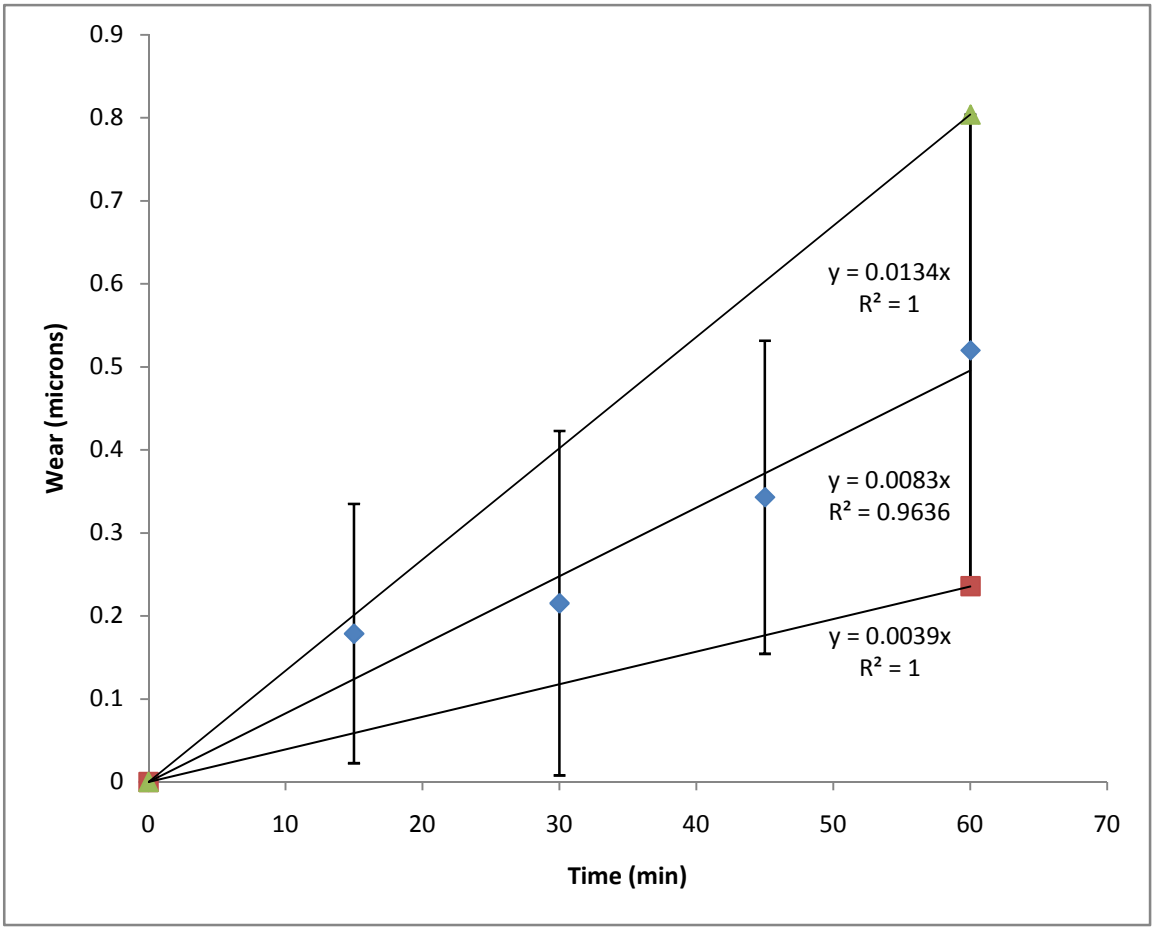

Figure 18. Metallic wear vs. time: 5 V DC, 25 Vpp

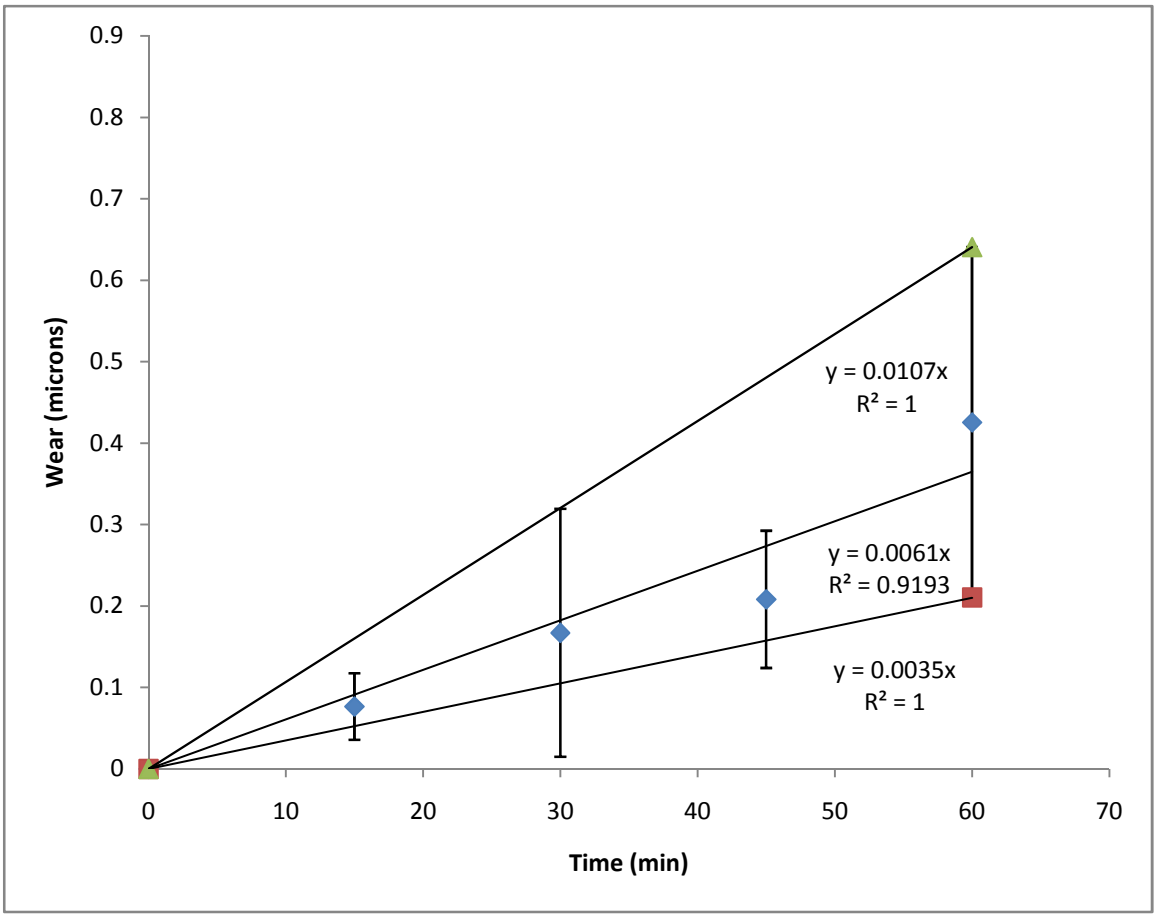

Figure 19. Metallic wear vs. time: 5 V DC, 30 Vpp

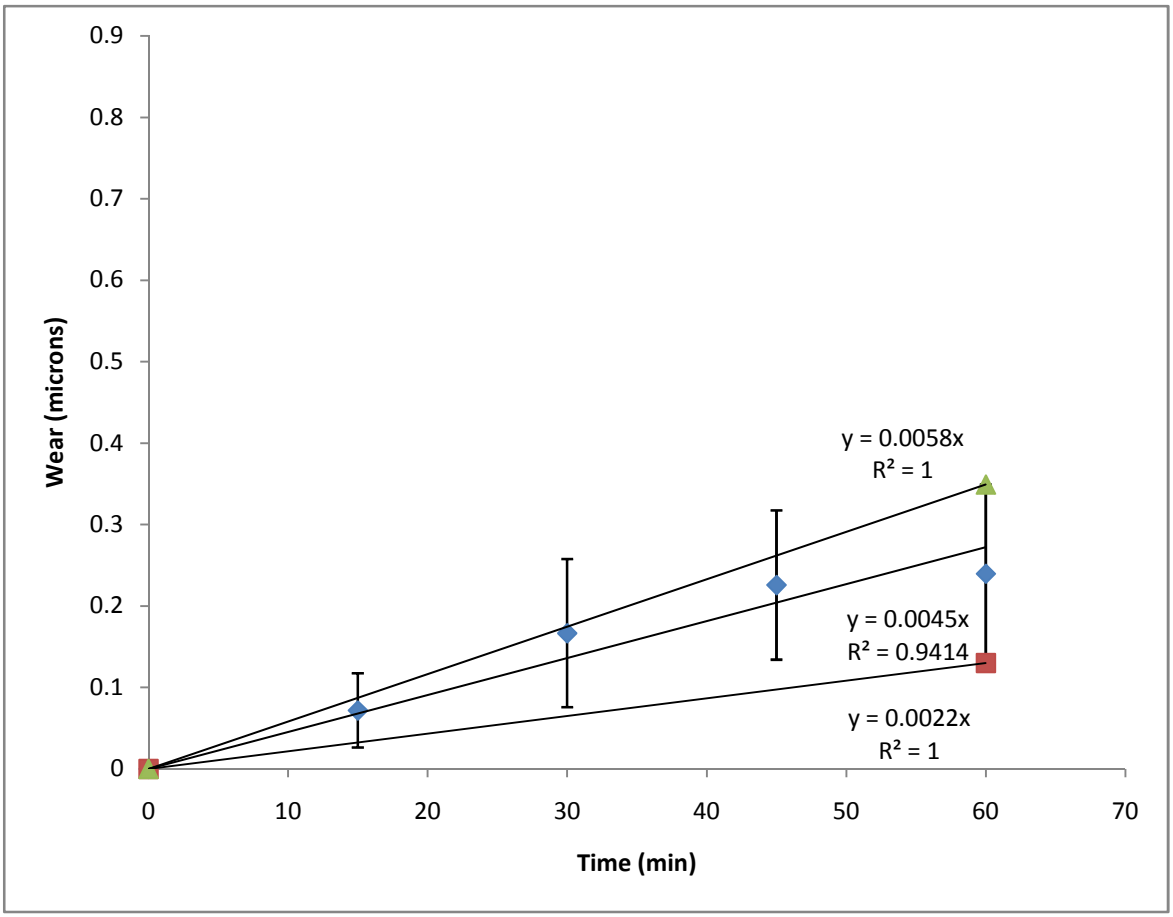

Figure 20. Metallic wear vs. time: 5 V DC, 35 Vpp

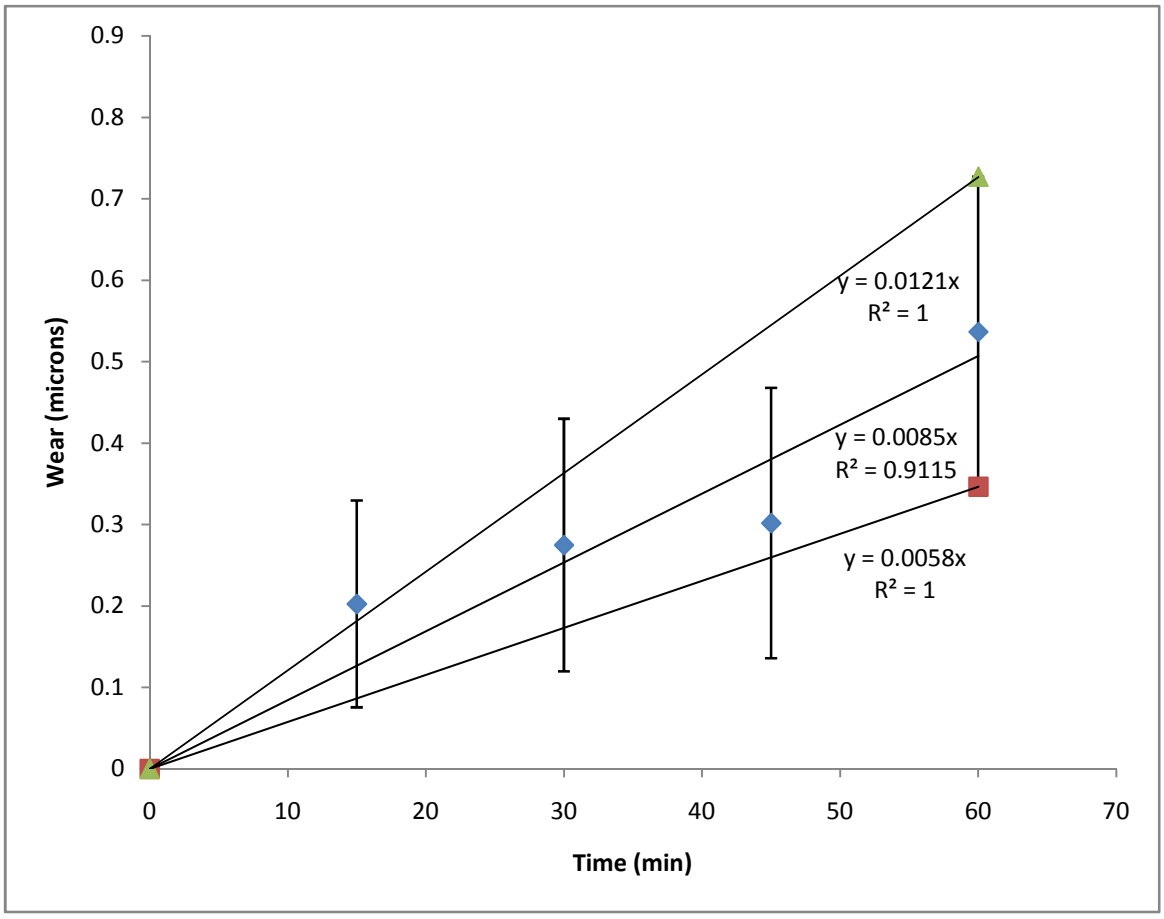

Figure 21. Metallic wear vs. time: 5 V DC, 40 Vpp

Table 7. Average, minimum, and maximum average experimental material removal rates for AC Voltages ranging from 0-40 Vpp.

AC Voltage (Vpp)	Avg. Exp. MRR (Å/min)	Min. Exp MRR (Å/min)	Max Exp. MRR (Å/min)
0	0	0	0
5	54	24	82
10	46	15	60
15	49	18	71
20	61	26	79
25	83	39	134
30	61	35	107
35	45	22	58
40	85	58	121

Discrepancies were still present in the data. For example, in Figure 14 the average wear data point for 30 minutes is lower than that of 15 minutes. Even though care was taken to ensure that line scans were taken on the same areas of each work-piece, it was impossible to ensure no error in the process. Therefore, data points which seem low were probably influenced by user error in performing the scans. There also could have been unknown variables in the process which caused data points to be lower than expected. Further investigation into defining such variables should be attempted in future work.

The goal of this thesis was to prove that the electro-kinetic process could be used to remove material from a metallic coated work-piece. The previous wear data proved that metallic material was removed from the work-piece surface. The material removal rate was predicted by equation 5.18 which is shown again below for convenience.

$$MRR = k_p V_{part\_x} P_o \tag{5.18}$$

In order to show the dependence of the electric field on the material removal rate, the maximum pressure was substituted into equation 5.19 which yielded:

$$MRR = k_p V_{part_x} \left(\frac{6\left(4a\varepsilon_r\varepsilon_o\zeta Ef(\kappa a) - 3v\eta d - 6\eta a\frac{dy}{dt}\right)E^{*2}}{\mu^2 R^2}\right)^{\frac{1}{3}} \tag{5.19}$$

Since the horizontal particle velocity and Preston's coefficient were constant, the maximum pressure was the only variable factor. The maximum pressure is directly proportional to the net normal force acting on the particle, which in turn is directly proportional to the amplitude of the AC signal. An approximation of the net force acting on a silica particle in the y-direction was found using equation 4.18. The values of the electrostatic, drag, normal, and net force acting on a particle in the y-direction are listed in Table 8.

Table 8. Numerical values of forces acting on a silica particle in the y-direction

AC Voltage (Vpp)	F_E (N)	F_N (N)	F_{drag_y} (N)	F_{net_y} (N)
0	8.35E-14	5.68E-15	3.60E-14	4.19E-14
5	1.25E-13	5.68E-15	3.60E-14	8.36E-14
10	1.67E-13	5.68E-15	3.60E-14	1.25E-13
15	2.09E-13	5.68E-15	3.60E-14	1.67E-13
20	2.50E-13	5.68E-15	3.60E-14	2.09E-13
25	2.92E-13	5.68E-15	3.60E-14	2.51E-13
30	3.34E-13	5.68E-15	3.60E-14	2.92E-13
35	3.76E-13	5.68E-15	3.60E-14	3.34E-13
40	4.17E-13	5.68E-15	3.60E-14	3.76E-13

Figure 22a shows that the net normal force increases linearly with an increase in AC Voltage. Figure 22b shows that the maximum pressure exerted on the work-piece surface also increases with increasing AC voltage. Since the material removal rate is directly proportional to the maximum pressure, the material removal rates should increase with increasing AC Voltage.

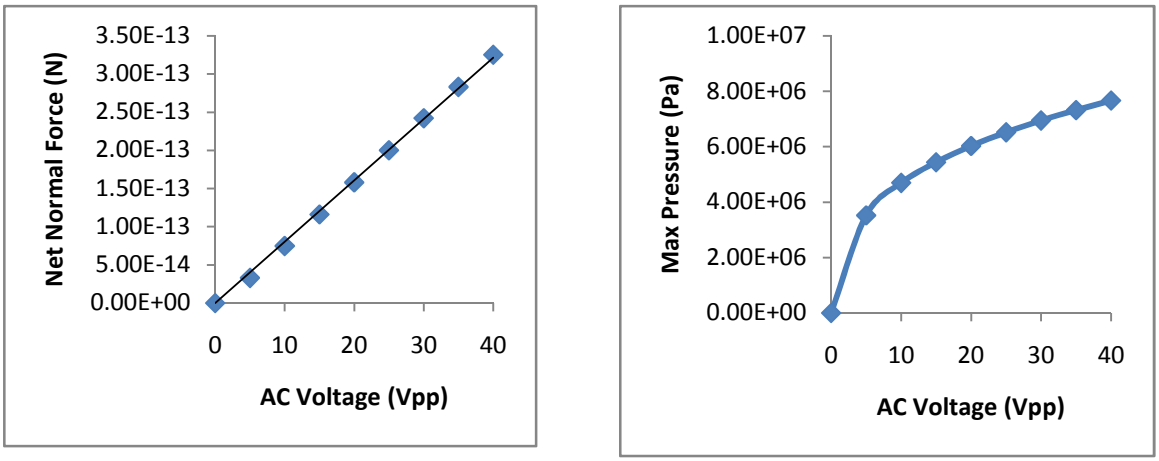

(a) (b)

Figure 22. The effect of AC Voltage on factors influencing the material removal process using the equations from the mathematical model and the constants listed in Table 5: (a) Net Force acting on a SiO_2 particle in the y-direction and (b) Maximum pressure exerted on the work-piece by a SiO_2 particle.

It was also desirable to control wear rates by adjusting the AC Voltage. From the force and pressure graphs from Figure 22, it was predicted that wear rate should increase with increasing AC Voltage. Figure 23 is a plot of the experimental and predicted average material removal rates vs. AC Voltage. The experimental average material removal rates are plotted as data points and the error bars represent the difference between those average data points and the minimum and maximum average material removal rates. These values were procured from the slopes of the trend lines in Figures 14-21 and were listed in Table 7. The predicted material removal rates were obtained from equation 4.22.

The predicted material removal rates increased with an increased AC Voltage. The experimental material removal rates followed this trend through 25 Vpp. Through the data point at 25 Vpp, the predicted and experimental material removal rates were very similar. However, experimental data points at 30, 35, and 40 Vpp displayed curious behavior. The experimental wear rates decreased for both 30 and 35 Vpp, and then increased significantly again at 40 Vpp. It was predicted that the wear rate should have continued to increase through 40 Vpp, however the particle visualization experiments shed some light on what could have caused the strange phenomenon following 25 Vpp. Recall from the particle visualization experiments that cavitation began to form in the micro-channel at 25 Vpp, and was significant at 30 Vpp. Wang et al. [23] reported that electrically-driven flow rates decreased significantly with increased cavitation in micro-channels. Therefore, it was reasonable that cavitation decreased the horizontal velocities of the SiO_2 particles which decreased the experimental material removal rates.

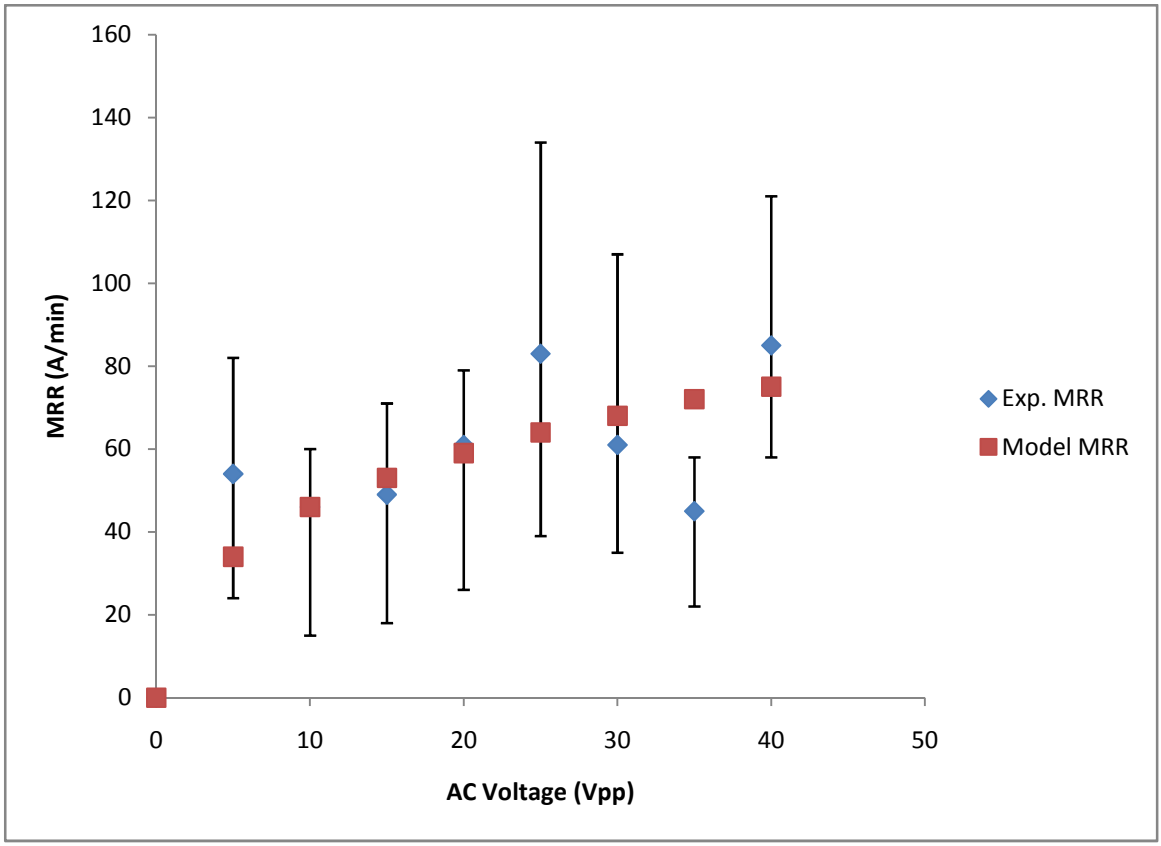

Figure 23. Experimental and predicted material removal rate vs. AC voltage

However, the decreased horizontal particle velocity does not explain why the experimental material removal rate increased at 40 Vpp. There could be a couple of different explanations as to what happened at the 40 Vpp data point. One explanation is that the bubbles began to burst at 40 Vpp. The energy released from bursting bubbles could have weakened and broken the gold and copper bonds at the surface which would have allowed the material to be easily removed.

A second explanation could be that galvanic corrosion was occurring at the work-piece surface which caused pitting to occur. Wranglen [24] stated that pitting is a localized attack, generally on dielectrics, which occurs due to the stimulation of the anode reaction by activating anions of the cathode reaction by the presence of oxidizing agents and by effective cathode surfaces with low polarization. A pit is initiated by the

absorption of activating anions on the defective sites in the dielectric. When the pitting potential is attained, the electric field strength above the thinnest parts of the dielectric will be so high that the anions will penetrate the film and a subsequent local dissolution of the gold surface might occur. Therefore, if pitting was occurring at the relatively high electric potential at 40 Vpp the experimental wear rates would be higher even if the wear caused by the mechanical removal process was decreased.

The model did not take into account the external factors which caused un-predicted material removal rates at AC voltages exceeding 25 Vpp. Beyond that point, the process was too unpredictable to accurately model. However, the model was effective at predicting material removal rates through 25 Vpp. The electro-kinetic process removed nano-metric amounts of metallic material from the work-piece surface and the process was effectively controlled over a range of 0-25 Vpp.

Chapter 7: Conclusions

The fundamental concept that electro-kinetically enhanced abrasive particles can remove metallic material from a silicon wafer substrate has been investigated experimentally and by numerical calculation. A micro-fluidic device was designed and fabricated in order to determine the effect that electric field has on particle motion suspended in solution and to prove that abrasive particles manipulated by an external electric field can remove metallic material from a silicon wafer substrate. A model based on the electrokinetic phenomena, particle force balance, Hertzian contact mechanics, and fluid mechanics was developed in order to determine theoretical material removal rates. The experimental and model results show agreement. The conclusions of this research are listed below.

- Applying a positive DC bias caused the negatively charged particles to move toward the work-piece, which was the positive electrode. Increasing the DC bias caused a greater percentage of the particles to reach the work-piece surface. DC biasing also caused particles to line up parallel with the side walls of the channel as a result of the concentrated electric potential at the channel side walls.
- Applying an AC voltage caused particles to exhibit a desired "blinking" motion which meant the particles were moving closer and further away to the work-piece surface through one period of the AC signal. Increasing the AC peak to peak voltage created more violent particle "blinking" and increasing the frequency caused the particles to blink more rapidly.

- Cavitation was seen at DC voltages exceeding 5 V and at AC voltages exceeding 25 Vpp. Material removal rates were undoubtedly affected when cavitation occurred.
- Area scans of the work-pieces which were subjected to material removal experiments exhibited material removal in line segments parallel to the side walls of the micro-fluidic channel. Metallic material was removed in this fashion due to the fact that the DC bias caused the particles to line up parallel to the side channel walls.
- Average metallic wear depth increased with time. Increasing the time allowed for the particles to remove material from more areas of the work-piece which increased the average wear depth. This was due to the fact that the line scans, which were perpendicular to the side channel walls, traced more removal areas on work-pieces influenced by material removal experimentation for longer periods of time.
- Average metallic material removal rates increased with increasing AC Voltage up to 25 Vpp. Increasing the AC Voltage caused an increase in the electrostatic force acting on each particle normal to the work-piece surface which increased the pressure that each individual abrasive silica particle exhibited on the work-piece surface.
- The experimental material removal rates and theoretical material removal rates predicted by the Hertzian model were in agreement up to 25 Vpp. Experimental material removal rates ranged from ~40-80 Å/min and theoretical material removal rates ranged from 34-75 Å/min over the specified range of AC voltages.

It is hypothesized that cavitation effects and galvanic corrosion led to the discrepancies of the material removal rates exceeding 25 Vpp. The model did not account for these effects due to a lack of predictability when these effects occurred.

References

[1] J.M. Steigerwald, S.P. Murarka, R.J. Gutmann. *Chemical mechanical planarization of microelectronic materials.* Wiley-VCH, Berlin, 1997

[2] Z. Wang, L. Yin, S.H. Ng, P.L. Teo. Chemical mechanical planarization. Technology Review, Singapore Institute of Manufacturing Technology. Available at http://www.simtech.a-star.edu.sg/research/TechnicalReports/TR0110.pdf

[3] T.H. Smith. Device independent process control of dielectric chemical mechanical polishing. Ph.D Thesis, Massachusetts Institute of Technology.

[4] J.T. Pan, P. Li, K. Wijeksoon, S. Tsai, F. Redeker. Copper CMP integration and time dependent pattern effect. *IEEE Interconnect Technology Conference,* 1999.

[5] D. Lim, I. Yoon, S. Danyluk. Effect of electric field on chemical mechanical polishing of langasite. *Wear,* 249:397-400, 2001

[6] G.S. Grover, H. Liang, S. Ganeshkumar, W. Fortino. Effect of slurry viscosity modification on oxide and tungsten CMP. *Wear,* 214:10-13, 1998

[7] G.H. Yost, W.S Williams. Chemomechanical effect in doped and intrinsic silicon. *Journal of American Ceramic Society,* 61:139, 1978

[8] A. Duboust, Y. Wang, F. Liu, W.Y. Hsu. Smoothly Does it. *European Semiconductor*, 2005

[9] Y. Mori, K. Yamauchi, K. Endo. Mechanisms of atomic removal in elastic emission machining. *Precision Engineering,* 10(1):24-28, 1988

[10] K. Yamauchi, K. Hirose, H. Goto, K. Sugiyama, K. Inagaki, K. Yamamura, Y. Sano, Y. Mori. First-principles simulations of removal process in EEM. *Computation Materials Science,* 14:232-235, 1999

[11] J. Bennett, J.J. Shaffer, Y. Shibano, Y. Namba. Float polishing of optical materials. *Applied Optics,* 26(4):696-703, 1987

[12] S.F. Soares, D.R. Baselt, J.P. Black, K.C. Jungling, W.K. Stowell. Float-polishing process and analysis of float-polished quartz. *Applied Optics,* 33(1):89-95, 1994

[13] M. Elimelech, R. Williams, J. Gregory, X. Jia. *Particle deposition and aggregation: Measurement, modeling, and simulation.* Butterworth-Heinemann, 1998

[14] J. H. Masliyah, S. Bhattacharjee. *Electrokinetic and colloid transport phenomena.* Wiley-Interscience, 2006

[15] G. Chen, P. Hui, K. Pita, P. Hing, L. Kong. Conductivity drop and crystallites redistribution in gold film. *Applied Physics A,* 80:659-665, 2005

[16] J. A. Fagan, P.J. Sides, D.C. Preive. Vertical oscillatory motion of a single colloidal particle adjacent to an electrode in an AC electric field. *Langmuir*, 18:7810-7820, 2002

[17] J. Li, P. Cheng. Bubble cavitation in a microchannel. *International Journal of Heat and Mass Transfer.* 47(12-13):2689-2698, 2004

[18] F.W. Preston. The theory and design of plate glass polishing machines. *J. Soc. Glass Technology.,* 11:214-217, 1927

[19] J. Luo and D.A. Dornfeld. Material removal mechanism in chemical mechanical polishing: Theory and modeling. *IEEE Trans. On Semiconductor Manufacturing,* 14 (2):112-133, 2001

[20] Y. Zhoa and L. Chang. A micro-contact and wear model for chemical mechanical polishing of silicon wafers. *Wear,* 252:220-226, 2002.

[21] S.H. Ng. Measurement and modeling of fluid pressures in chemical mechanical polishing. Ph.D Thesis. Georgia Institute of Technology.

[22] K.L. Johnson. *Contact Mechanics*. Cambridge University Press, New York, 1985

[23] M. Wang, J. Wang, S. Chen. Roughness and cavitations effects on electo-osmotic flows in rough microchannels using the lattice Poisson-Boltzmann methods. *Journal of Computational Physics,* 226:836-851, 2007

[24] G. Wranglen. *An Introduction to Corrosion and Protection of Metals.* Chapman and Hall, London, 1985